TITLE PAGE

TITLE

Mouse navigation strategies for odor source localization

RUNNING TITLE

Odor source localization by mice

AUTHOR NAMES AND AFFILIATIONS

Liu, Annie[1,4*], Papale, Andrew E[1*], Hengenius, James[2*], Patel, Khusbu[3], Ermentrout, Bard[2,4], and Urban Nathaniel N[1,4]

[*] These three authors contributed equally to this manuscript

1. Department of Neurobiology, University of Pittsburgh School of Medicine, Pittsburgh, PA
2. Department of Mathematics, University of Pittsburgh, Pittsburgh, PA
3. University of Pittsburgh, Pittsburgh, PA
4. Center for the Neural Basis of Cognition, Pittsburgh, PA

AUTHOR CONTRIBUTIONS

JH, AL, BE, and NNU designed the behavioral experiments. AEP, JH, BE, and NNU designed the simulations. AL and KP conducted the behavioral experiments. AEP, JH, and AL analyzed the data. AEP and JH wrote the MATLAB code. AEP calculated the statistics. AEP, JH, AL, BE, and NNU wrote the paper.

CORRESPONDING AUTHOR

Andrew E. Papale

papalea@pitt.edu

KEYWORDS

Olfaction, navigation, casting, binaral-olfaction, binaral-sniffing, serial-sniffing

SUMMARY STATEMENT

Use of a naturalistic odor-source localizing task uncovers key strategies underlying successful mouse navigation. Concentration-dependent models successfully recapitulate mouse behavior and reveal important behavioral components.

ABSTRACT

Navigating an odor landscape is a critical behavior for the survival of many species, including mice. An ethologically relevant mouse behavior is locating food using information about odor concentration, such as the relatively laminar gradient established by diffusion-convection near surfaces. To approximate this behavior, we use an open field odor-based spot-finding task indoors with little wind, examining navigation strategies as mice search for and approach an odor source. After mice were trained to navigate to odor sources paired with food reward, we observed behavioral changes consistent with localization 10-45cm away from the source. These behaviors included both orientation towards the source, decreased velocity, and increased exploration time. We also found that the amplitude of 'casting,' which we broadly define as lateral back and forth movement of the olfactory sensors, increased with proximity to the source. Based on these observations, we created a concentration-sensitive model to simulate mouse behavior. This model provided evidence for a binaral-sniffing strategy (inter-nostril comparison of concentration in a single sniff) and a serial-sniffing strategy (sampling concentration, moving in space, and then sampling again). Serial-sniffing may be accomplished at farther distances by moving the body and at closer distances by moving the head (casting). Together, these results elucidate key components of behavioral strategies for odor-based navigation.

INTRODUCTION

Mice, insects, and other animals navigate odor trails and locate odor sources with high fidelity, a remarkable feat given the complexity and variability of odor stimuli. Prior studies of olfactory navigation have focused on the mechanisms of navigating through odor plumes in air (Gire et al., 2016; Vickers, 2000) or water (Koehl et al., 2001), or of scent-tracking on the ground, specifically following odor trails (Khan et al., 2012; Means et al., 1992; Porter et al., 2007; Thesen et al., 1993; Wallace et al., 2002). However, different strategies may emerge for search under conditions near surfaces where intermittency (the fraction of samples above detection threshold) is high (Connor et al., 2018). In this study, we examine the odor-driven behaviors involved in the search for a discrete

odor object under low wind conditions where gradient information is preserved, and develop a model of olfactory navigation to describe multiple strategies used for effective odor localization.

One general navigation strategy preserved across species and environmental conditions involves the use of lateral back-and-forth changes in orientation of the olfactory sensors during active odor-sampling (Baker et al., 2018). Moths navigating odor plumes use this strategy to reacquire an odor plume, a behavior termed “zig-zagging” or “casting” depending on the magnitude and angle of displacement (Carde & Willis, 2008; Kennedy, 1983; Kuenen & Carde, 1994; Marsh et al., 1978). Flies (Budick & Dickinson, 2006) and cockroaches (Willis et al., 2008) use a similar casting strategy during plume navigation. Lateral back-and-forth behaviors are also often observed in animals following odor trails. Rats employ head oscillations that sweep back and forth across a trail as they track it (Khan et al., 2012), a strategy also used by humans (Porter et al., 2007) and ants (Draft et al., 2018; Hangartner, 1969) following trails. In this study, we use the term ‘casting’ to describe the amplitude of the movement of the olfactory sensors during navigation toward an odor source (Baker et al., 2018; Zhao et al., 2017).

Successful navigation of a complex odor environment likely involves different behavioral strategies at different times. Knowledge of the odor environment, characteristics of specific odor cues, and general task context may each influence odor-guided behavior. Animals demonstrate strategy-switching between distinct behaviors as a consequence of both changes in odor stimulus properties and task context (Gire et al., 2016; Pierce-Shimomura et al., 1999; Thesen et al., 1993; Wesson et al., 2008). Environmental familiarity and visual cues also influence decision-making strategy during odor source localization. Given visual cues to navigate, exploratory casting based on odor cues disappears on tasks with a small number of potential goal locations; instead, mice begin directly navigating to known odor source locations in straight-line trajectories (Bhattacharyya & Bhalla, 2015; Gire et al., 2016). This resembles the transition from exploration to exploitation behavior observed during successive search trials (Hills et al., 2015; Sutton & Barto, 1998). Thus, both behavioral context and the availability of orienting stimuli are important for strategy choice in odor source localization.

Here, we use an open field odor-based spot-finding task to examine strategies of olfactory search for an odor source deposited on the surface under air flow conditions typical of an indoor setting. By randomizing odor source location, performing experiments in the dark, and using a discrete

target odorant object, we prevent mice from switching to methods of systematic search based on memory, visual, or proprioceptive cues (Gire et al., 2016). We find that multiple dimensions of behavior are varied as mice approach the odor source, including velocity and casting, suggesting that these behaviors are associated with odor detection or localization. We then created agent-based models of olfactory search and use simulations to interrogate the roles of binaral-sniffing, variable velocity, and variable casting on effective odor localization. Both behavioral and simulation data suggest that multiple behavioral strategies are important for successful odor navigation to a deposited odor source under typical indoor air flow conditions in mice.

MATERIALS AND METHODS

Ethical approval. All experiments were completed in compliance with the guidelines established by the Institutional Animal Care and Use Committee of the University of Pittsburgh.

Animals. Four male and one female adult M72-IRES-ChR2-YFP knock-in mice (The Jackson Laboratory) (N=5) were used for this study, with training begun after age P47. Average age at training start was P72. All mice were housed singly with behavioral enrichment (running wheel and house) and received unlimited access to water in their home cage.

Behavioral arena. A large, open field behavioral arena was used for data collection, as described in Jones and Urban, 2018 (Figure 1A, adapted with permission from Jones and Urban, 2018). The arena is a custom built 36” x 45” transparent plexiglass and acrylic surface without walls mounted 4 feet above the floor in an aluminum frame. Rows of infrared light-emitting diodes (LEDs) were mounted along each of the four table surface edges. Data were collected using a camera mounted below the table surface (1280x1024 resolution, 11.2pixels/cm, 50 frames s^{-1}, Flea3, Point Grey Imaging). Trials were run in the dark and LEDs from equipment in the room were blacked out with electrical tape. Remaining light from computer monitors was red-shifted so as to not be visible to the mice.

Odorized crayon. We created odorized wax crayons similar to what was described in Jones and Urban, 2018. Briefly, 4.9 g of a Crayola crayon, 0.1 g of Crayola chalk, and 0.1 g of odorant consisting of one of three different concentrations (0.1%, 1%, and 2% by weight) of methyl salicylate (Sigma-Aldrich) diluted in mineral oil (Fisher Chemical Paraffin Oil, 0121-1) were mixed

together, and the mixture was poured into a silicon or rubber crayon mold. After ten minutes, the mixture cooled and hardened into an odorized crayon.

Task: Prior to each trial, the table was wiped clean with 200 proof ethanol using a paper towel. After the table dried, a spot ~1cm in diameter was drawn in a pseudorandom location in the central area of the table (Figure 1B). Based on recent spot placements, the experimenter attempted to place the spot at a different location each subsequent trial. For baited trials, a small piece of chocolate or peanut (~0.1 g) was placed in the middle of the spot, while for unbaited trials, the spot was left empty. No more than 2 unbaited trials were run on a given day to prevent extinction of motivated behavior. With the lights off, a mouse was placed onto the table at a pseudorandom starting location along the right side of the table and allowed to freely explore the arena for approximately 3 minutes. Over the course of 5 months, 133-197 trials were collected per animal, 3-5 trials per day, 3-5 days per week, at a time between 9 am and 2 pm on a normal light-dark cycle.

Food deprivation and task training. To motivate mice to perform the task, they were food deprived to 78±07% of original body weight. Animals received between 1.8-2.2 g of their normal chow per day and were given free access to water. Animals were trained to associate a spot of odor (<1cm diameter) with food reward, either a small sliver of peanut or milk chocolate. Training consisted of two stages over the course of 7-10 trials: 1) habituation (2-3 days); and, 2) odor-reward association (5-10 days). During habituation, mice were placed on the table for one 15 minute long trial on two consecutive days and allowed to explore the arena with no food reward present. During initial food-odor association, plexiglass dividers were used to decrease the arena size to 25% of the full arena. A baited odor spot was placed on the table. Once animals found the baited spot in the small arena during at least 66% of the day's trials, the arena size was increased to 50% the size of the full arena, followed by an increase to the full 45" x 36" arena once the spot was again found during 66% of the day's baited spot trials. Unbaited spot finding trials were introduced only after the animals successfully performed the baited spot task in the full arena. Training ended and data collection began upon successful performance of unbaited spot trials, which occurred following 6-13 days of training (18-39 trials). All reported data are from the full sized arena, but contain both baited and unbaited trials. Baited and unbaited trials were analyzed separately, but were found to be qualitatively similar and so are grouped together.

Video Processing. 44 trials were removed from analysis for technical reasons, leaving N=915 trials analyzed. Trials were removed if 1) the video file was corrupted; or, 2) tracking the mouse using Optimouse (see below) was judged by the experimenter to be unsuccessful before data analysis began. This likely occurred due to unintended variation in table illumination on different trials. Of these 915 trials, 54 had odor spot placement within 4 cm of the edge, and were removed from further analysis due to potential obstruction of mouse trajectories near the spots. Finally, 5 trials were removed because the mouse found the spot within 1 s, indicating that it was initially placed on the arena too close to the odor spot (most trials where this occurred the mouse started within 10 cm of the odor spot). This left N=853 trials analyzed here. Raw avi formatted files were processed using the Optimouse open source program (Ben-Shaul, 2017) to extract body position and nose position. Extracted position files were then post-processed with in-house software written in Matlab (www.mathworks.com). Position frames were then passed through a 5th order median filter to suppress jitter in the position data and remove high-frequency noise. Position data was excluded if 1) Optimouse failed to detect a position, 2) the $\log_{10}$ of mean mouse brightness was less than 0.5 times the mean for that trial, 3) if mean velocity was greater than 100 cm s^{-1}, 4) if the mouse length was greater than 8 cm, 5) if the mouse position 'jumped' by more than 35 pixels (3.13 cm) between consecutive frames, and 6) if the mouse position was 4 cm or closer from the edge of the arena. Note that the edges of the arena were metal fasteners and the mouse was often partially obscured from below when it walked around the edges. Exclusion criteria 6) accounted for the majority (N= 6E6; 84%) of excluded frames, as mice spent a good deal of time at the edges of the arena. Finally, a nearest neighbor filter was used to remove times when the mouse was stationary as the computation orientation of the mouse was unstable here. For the majority of analyses, we focused on either the time before a spot was found, or a matched sample of times for unsuccessful trials.

Behavioral Analysis. A successful spot trial was scored when the mouse's nose came within 1.5 cm of the spot, based on a sharp increase in the survival function on minimum distance to the spot (Figure 2A).

The fraction of the arena explored was calculated by binning the arena into approximately equal-area parts of 9-10,000 partitions and, then, the percentage of time exploring the center of the arena (excluding 4 cm around the edges) was calculated.

Analysis of percent exploration time entailed defining 100 circular rings around the odor spots at intervals of 1 cm. The number of samples in each ring was then normalized by the total number of samples in the trial to (% time). For trials when the mouse failed to find the odor source, the entire session was used.

To compute the probability of successfully finding an odor source as a function of distance, the occupancy was divided into successful trials (hits) and unsuccessful trials (misses). The fraction of hits was divided by the total number of trials (hits + misses) and averaged across mice.

The orientation relative to the odor spot was calculated by computing the difference in the four-quadrant arctangent of the vectors from body-to-nose and body-to-spot (Figure 3E).

Derivatives were computed using the adaptive windowing Janabi-Sharifi algorithm (Janabi-Sharifi et al., 2000) available online (Manurung, 2016), but modified to handle missing data points (NaNs) and to allow for post-smoothing. Parameters used were a window size of 50 (1 s) and an error term of 0.2, with post smoothing of 0.1s.

Casting behavior was quantified by computing the numerical derivative of the arctangent of the nose velocity, taking the absolute value, and then dividing by the linear velocity of the nose (|dPhi|/nV). This is a modification of the zIdPhi measurement (Papale et al., 2012). |dPhi|/nV is equivalent to the signed curvature formula with units of m^{-1} and is therefore an appropriate measure of tortuosity. The algorithm was extensively tested on variable-frequency sine waves to verify that segments of high curvature were well-separated from segments of high linearity across a wide range of frequencies. Then, for position data from mice, the $\log_{10}$ of the absolute value of |dPhi|/nV was taken to generate a roughly normal distribution. An example of the |dPhi|/nV casting measure (Figure 1C) for one analyzed behavioral trial shows ‘elbows’ and angled segments with high curvature (black arrow) well-separated from straight segments of high linearity.

An alternate measure of casting used was the angle of the nose relative to the midline. For this measure, the angle from the nose to the midline was determined by calculating a vector for the mouse’s current heading and computing the shortest distance from the detected nose point to that line, then taking the arccosine of that angle.

Anemometer Measurements. A hot wire anemometer (TSI Velocicalc 9535A) was placed at 9 different positions across the table (Figure 1D). 10 measurements were taken with the sensor aligned to the long-axis or short-axis of the table at each position and the respective averages were taken.

PID Measurements. A cotton swab dipped in 99% Methyl Salicylate liquid was placed at the center of the table (Figure 1D, gold star) at approximately 0.5cm from the surface. Concentration was measured for 30s at distances from 0.5cm to 15cm using a Photoionization Detector (PID) (miniPid, Aurora Scientific). Raw measurements had noise peaks at 60Hz and 72Hz, broad spectrum high frequency noise, and substantial baseline drift. To remove the noise peaks, two 2nd order Butterworth IIR notch filters were used. To remove high frequency noise, a (0.2s backward, 0.02s forward) moving mean filter was used. To remove baseline drift, a baseline estimation and denoising function was used (Duval, 2018). The denoised traces (Figure 1E) show large signal fluctuations and, generally, decreasing mean output with distance. Intermittency was calculated as the mean number of points greater than a threshold of 0.005.

Shuffled Spot Control. As a control, spots were randomly shuffled and paired with tracking data from one session. Shuffled spots had to be at least 5cm away from the original spot. Analyses were repeated with the shuffled control data.

Model Specification. Based on observations of mouse behavior, we developed an agent-based model that navigated a virtual odor environment. This agent made temporally discrete sniff-to-sniff comparisons of odor concentration as it moved through virtual space, altering its heading toward higher concentrations and away from lower concentrations. The agent consisted of a body with coordinates (x, y) and moved through space along a heading θ at a velocity v_c:

$$x_{t+\Delta t} = x_t + v_c\, \Delta t \cos\theta \tag{n1}$$

$$y_{t+\Delta t} = y_t + v_c\, \Delta t \sin\theta \tag{n2}$$

where Δt=0.1 s represents a constant the inter-sniff interval. The agent's nose was located at a distance ℓ=5 cm from the body at coordinates (x_n, y_n). The nose was further divided into left and right nares, (x_{nL}, y_{nL}) and (x_{nR}, y_{nR}), separated by an inter-nares distance, d_{nares}=1.8 mm. The two nares are separated by an angle 2γ. The nose was capable of limited movement independent of the body heading, with an angular deflection ϕ relative to the forward heading. Nares positions were given as:

$$x_{nL/nR} = x + \sqrt{l^2 + \left(\frac{d_{nares}}{2}\right)^2} \cos(\theta + \phi \pm \gamma) \quad \text{(n3)}$$

$$y_{nL/nR} = y + \sqrt{l^2 + \left(\frac{d_{nar}}{2}\right)^2} \sin(\theta + \phi \pm \gamma) \quad \text{(n4)}$$

with nose deflection bounded within ± ϕ_{max} as dictated by mouse anatomy. The agent geometry is shown superimposed on a mouse body (Figure S2A).

The independent motion of the nose is what allows the agent to sample concentrations to the left and right of its current heading and adjust its heading toward higher concentrations (Figure 5C). The distribution of observed mouse nose deflections was approximately Gaussian (Figure S2C); therefore, we modeled the angular movement of the nose as an Ornstein-Uhlenbeck (OU) process, a mean-reverting correlated random walk with a Gaussian stationary distribution. At each sniff, the nose deflection was updated according to:

$$\phi_t = \phi_{t-\Delta t} - \frac{\phi_{t-\Delta t}}{\tau}\Delta t + dW_t\sqrt{\frac{\Delta t}{\tau}} + \tanh\left(k_{binaral}(c_L - c_R)\right)\Delta t \quad \text{(n5)}$$

$$dW_t \sim N(0, \sigma_c^2) \quad \text{(n6)}$$

$$\sigma_c = \sigma_{min} + (\sigma_{max} - \sigma_{min})\frac{C_t}{k + C_t} \quad \text{(n7)}$$

where τ is the characteristic time constant of the process, σ_c is the concentration-dependent standard deviation of the nose deflection, dW_t is a normally distributed random variable with mean of zero and standard deviation σ_c. To this OU process, we add binaral bias in the form of the hyperbolic tangent of the left-right concentration difference; when $C_L > C_R$, the nose is biased to the left and *vice versa*. Here, $k_{binaral}$ controls the response of the nose to binaral inputs. The concentration value C_t is the average concentration across both nares at time t:

$$C_t = \frac{(c_L + c_R)}{2} \quad \text{(n8)}$$

Here, c_L is the concentration at the left naris and c_R is the concentration at the right naris.
We observed that mouse speed increases with distance from the odor source (see Figure 3F). Because the agent in our model does not have information about its distance from the odor source, instead we used a concentration-dependent modulation of speed. Specifically, we use a sigmoidal function with a quartic coefficient to approximate concentration-dependence of speed:

$$v_c = v_{max}\left(1 - \frac{C_t^4}{k + C_t^4}\right) \quad \text{(n9)}$$

where v_{max} is the maximum velocity and k=½ concentration units. Note that this is the same k that appears in eq n7.

Model Odor Environment. The agent must iteratively sample concentrations in an odor environment to navigate in the direction of higher concentration. To simulate the ambient concentration, *C(x,y),* we use a noisy bivariate exponential distribution normalized to a value of one at the source:

$$C(x,y) = e^{-\left(\frac{\sqrt{(x-x_{sp})^2+(y-y_{sp})^2}}{2\,\sigma_{sp}^2}\right)}(1+\eta) \quad \text{(n10)}$$

$$\eta \sim U(-k_n, k_n) \quad \text{(n11)}$$

Here, (x_{sp}, y_{sp}) is the location of the source, σ_{sp} controls the width of the odor distribution around the source (model results were obtained with σ_{sp}=20 cm), and η is multiplicative uniform noise added to each point in a spatial grid to approximate the effect of turbulent flow, bounded at k_n=0.5.

To represent the table, we generate a static smooth odor landscape grid with a resolution of 1 mm according to eq n10 (Figure 5B, step 1). Next, we then apply noise according to eq n11 (Figure 5B, step 2). We then simulate the PID intermittency in the odor signal by randomly setting grid values to zero (Figure 5B step,3). The probability that a grid value is zeroed, P_{int}, increases with distance from the source according to

$$P_{int} = 1 - e^{k_{int}\sqrt{(x-x_{sp})^2+(y-y_{sp})^2}} \quad \text{(n12)}$$

where k_{int} is the decay parameter set to -0.002 cm^{-1}. Finally, we apply a Gaussian filter with a standard deviation of 4 mm to introduce local spatial correlations into our landscape (Figure 5B, step 4).

To reflect the apparent lack of mouse orientation toward the source beyond 30 cm, (Figure 3D), the models have a concentration detection threshold of 0.25 concentration units. This represents a distance of approximately 30cm from the source.

A distribution of simulated spot positions was used for simulations, matched to data (Figure 1B), but due to edge effects reducing overall model performance, spots closer than 10cm to the walls were not used.

Concentration-Sensitive Model (CSM). The agent moves along forward heading θ at velocity v_c, iteratively sniffing the concentration at its nose coordinates (Eqs n1-n4). At each sniff, the agent's nose randomly samples to the left or right of the forward heading depending on the state of the

random nose deflection process (Eqs n5-n7). It compares the current concentration sample, C_t, to the sample from the previous sniff, $C_{t-\Delta t}$. If C_t is greater than $C_{t-\Delta t}$, the agent sets its heading to the direction of the nose, $\theta_{t+\Delta t} := \theta_t + \phi_t$. If C_t is less than or equal to $C_{t-\Delta t}$, the agent turns away from the direction of the nose, $\theta_{t+\Delta t} := \theta_t - \phi_t$. This algorithm is effective at reproducing key parameters of mouse odor source localization (Figure 5):

$$\theta_{t+\Delta t} = \theta_t + \phi_t \; if \; C_t > C_{t-\Delta t} \;\; else \; \theta_t - \phi_t \; if \; C_t \leq C_{t-\Delta t} \qquad \text{(n13)}$$

Correlated Random Walk (CRW) Controls. To test model behavior in the absence of odor-sensitivity, and to serve as a control in case mice were randomly finding the spots, concentration-dependent turning was removed from the model and replaced by a random turning decision. Eq n13 is replaced by:

$$\theta_{t+\Delta} \; = \theta_t + \phi_t \; if \; z > 0.5 \;\; else \; \theta_t - \phi_t; \;\; z \sim U(0,1) \qquad \text{(n14)}$$

To our surprise, CRW control models had a similar success rate to mice when run for 180 s. After observing mice on videos; however, we determined they were not exploring the arena for the entire 180 s trial. On successful trials, before finding the odor spots, the average time mice actually spent exploring the center of the arena was only ~30 s. The CRW controls continuously explored the center of the arena as their decision rule at table boundaries was to bounce off like a billiard ball. Therefore, we ran all simulations for 30s to match average mouse exploration time in the center of the arena.

Reduced Model Controls. To evaluate the effects of different hypothesized features of mouse navigation, we constructed 8 model variant combinations by leaving out binaral-sniffing, concentration-dependent velocity, and/or concentration-dependent casting amplitude. We then evaluated CSM model performance in the absence of these features. To eliminate binaral-sniffing from the model, $k_{binaral}$ in eq n5 was set to zero. To remove concentration-dependent velocity from the model, eq n9 was modified so that v_c was equal to the constant v_{max}. To remove concentration-dependent casting amplitude from the model, eq n7 was modified so that σ_c was set equal to the constant σ_{min}. The same 8 model variants were created for the CRW control, and results were averaged together to obtain a control distribution (Figure 6, black lines; Figure 7A, grey bar).

355

356 **RESULTS**

357 *An open field odor-based spot-finding task was developed.*

358

359 To examine the behaviors relevant to odor source localization, we designed a task that minimized
360 non-olfactory cues. Five mice were trained to find a <1cm diameter spot of odorized wax within a
361 rectangular behavioral arena of approximately $1m^2$ in the dark (Figure 1A, and Methods). Odor
362 sources (methyl salicylate with(out) bait) for each of the trials (N=855) across all mice (N=5) were
363 pseudo randomly distributed within the center of the testing table (Figure 1B). An example
364 trajectory shows the nose position of the mouse starting at the right-hand side of the arena and
365 moving leftward before successfully finding the spot (red circle; Figure 1C). In this figure, the color
366 indicates a measurement of curvature (|dPhi|/nV; see Methods) used to detect casting amplitude.
367 Additional example trajectories are displayed in Figure S1, with color indicating relative time (in
368 seconds).

369

370 *Wind Conditions in the Room.* We did not generate any airflow during these experiments but of
371 course air flow occurs in every typical environment and air movement likely dominates the effects
372 of odor diffusion in the vast majority of environments. The room in which these behavioral data
373 were acquired had a ventilation input vent at roughly the center of the room and the primary outflow
374 in the room was underneath the door. Airflow measurements were taken on the behavior table
375 (height 1.135m above the floor) at 9 positions and 2 orthogonal orientations. Wind speed was
376 measured between 1.9ft/min – 9.6ft/min along the short axis and 9.2ft/min – 35.1ft/min along the
377 long axis of the table (Figure 1D). Wind direction was estimated by taking the four-quadrant
378 arctangent (green arrows).

379

380 *Photoionization Detector (PID) Measurements on Behavior Table.* A cotton swab dipped in 99%
381 methyl salicylate was placed at the center of the table (Figure 1D, gold star). The tip of a PID was
382 placed at distances from 0.5cm to 15cm away from the odor source. After denoising (see
383 Methods) PID traces were highly variable but mean output decreased reliably with distance (Figure
384 1E). Three aspects of the PID data were characterized. The mean variance increased for
385 distances less than 2.5cm and then decreased (Figure 1F, left panel). The increase at small
386 distances could be due to saturation of the PID at high concentrations. The mean output also
387 decreased with distance from the source from about 2.5cm (Figure 1F, center panel).

388 Intermittency was measured as the fraction of samples above baseline, and decreased with
389 distance from the source (Figure 1F, right panel).
390
391 *Mice learn the open field odor-based spot-finding task.* To determine an appropriate distance
392 threshold for achieving a successful trial and an approximate minimum concentration-detection
393 threshold, we examined the survival function with respect to distance from the spot (Figure 2A).
394 Typically, a survival function is used to determine the probability that a variable of interest survives
395 past some time point; here, we use it to describe the probability of a mouse reaching a given
396 distance away from the odor spot. For mice, there was a sharp increase in survival at about ~1.5
397 cm, with a more gradual increase toward 100% at about 90 cm from the odor spot (red line). Thus,
398 mice on all trials successfully came within ~90 cm of the spot. In contrast, the survival function
399 from shuffled data rose smoothly, crossing the mouse data at about 30cm. We therefore set the
400 distance threshold for finding a spot to be 1.5cm and estimated the minimum concentration-
401 detection threshold to be 30cm for later modeling purposes.
402
403 Given a threshold of 1.5cm, mice were successful in 64% (N=532/826) of trials (Figure 2B). In
404 comparison, shuffled controls were successful a mere 1.67% (N=1,524/91,446). Mice had a
405 significantly higher success rate than shuffled controls (Welch's t-test; p=6.22E-5, t-stat=14.69,
406 df=4). A logistic regression on successful versus unsuccessful trials for mouse data revealed
407 several highly predictive explanatory variables (Table S1). Baited trials had higher success rates
408 (p=4.68E-12, β=2.51), potentially indicating higher motivation during these trials or a contribution of
409 the odor of food to the localization. Greater arena exploration also predicted success (~45 cm^2
410 bins; p=1.65E-15, β=15.51; see Figure 3A). Slower mice (p=6.89E-06, β=-0.29) were more
411 successful, though they had faster average nose velocity (p=1.07E-04, β=0.27) and higher casting
412 (integrated $\log_{10}$[|dphi|/nV] within 30cm; p=2.56E-3, β=1.4), suggesting that slower forward body
413 velocity and higher casting amplitude may be features of successful search strategies. Successful
414 completion of this spot-finding task is thus dependent on features of individual trajectories.
415
416 We conclude that mice find odor spots above chance levels established by the shuffled control,
417 and predict that further evaluation of specific trajectory features will provide useful information
418 about odor localization strategy.
419
420 *Mice efficiently navigate to the odor source in comparison to shuffled controls.*

421

422 Next, we compared navigation efficiencies of mice to data from shuffled controls by examining time
423 to spot divided by initial distance, nose displacement divided by initial distance, and the probability
424 of finding the spot as a function of distance. Time to spot was divided by initial distance to spot,
425 with the average for mice (0.51 s/cm) significantly lower than shuffled controls (1.71 s/cm; Figure
426 2C; Welch's t-test; p=7.25E-18, t-stat=8.72, df=1700). Then, nose displacement was divided by
427 initial distance to spot, with the average for mice (4.75x) significantly lower than shuffled controls
428 (17.78x; Figure 2D; Welch's t-test; p=1.2E-19, t-stat=-9.11, df=1573). To determine the probability
429 of finding the odor source at various distances away, successful samples (spot found) were divided
430 by total samples (spot found + not found) in concentric annuli centered at the spot (Figure 2E). For
431 mice, this resulted in a fairly linear distribution (red line), while for shuffled controls the distribution
432 was highly nonlinear (cyan line). We conclude that mice are more efficient at navigating to the
433 odor source than shuffled controls.

434

435 *Mouse behavior varies systematically as a function of distance from the odor source.*

436

437 As suggested by the logistic regression analysis of mouse data, exploration percentage, velocity,
438 and casting amplitude are important for odor source localization. Next we tested whether mice
439 reliably change behavior depending on proximity to the odor source. We conducted four analyses
440 to test this hypothesis: 1) looking at the percentage of the arena explored, 2) computing the
441 percentage of time exploring at a given distance on a given trial; and separately, 3) examining
442 mouse velocity as a function of distance from the odor source; and 4) analyzing mouse heading
443 relative to the odor source.

444

445 Using a bin size of ~45 cm^2, mice explored an average of 33±17% (mean±s.d.) of the table before
446 finding the spot. This estimate varied as a function of bin size and successful spot-finding (Figure
447 3A; two-way ANOVA interaction term; p<1E-100, F=83.95, df=97). Mice also explored
448 progressively less of the table with increasing trial (~45 cm^2 bins; ANOVA; p=2.65E-51, F=57.16,
449 df=5), suggesting refinement of learning throughout the experiment.

450

451 We then computed the percentage of time mice occupied different distances from the odor source,
452 normalized by the area of the annulus (Figure 3B). This revealed a decreasing function with
453 distance on successful trials (red line) compared to a flat distribution with distance on unsuccessful

trials (blue line). These lines diverged at a distance of 44cm (two sample Kolmogorov-Smirnov test; $p<1E-10$), suggesting that mice are exploring more within 44cm of the odor source on successful trials.

Next, we examined mouse velocity as a function of distance from the odor source (Figure 3C). As mice approached the odor source across all trials, nose velocity slowed down (ANOVA; p=2.72E-91, F=18.73, df=28), as did body velocity (ANOVA; p=1.02E-160, F=31.12, df=28).

We next examined mouse heading relative to the odor source for successful trials (Figure 3D). If a mouse detects odor cues that provide insight into the location of the odor source, then the mouse's nose should orient towards the source. At each position sample, the difference in angle between body-to-spot and body-to-nose was computed (Figure 3E). We found that orientation relative to the spot depended on distance from the odor spot (Watson-Williams Test; $p<1E-100$, F=877.94, df=48), and has a median value not significantly different from zero (i.e. oriented directly at the spot) within 9.54cm ($p>1E-3$, circular test for equal medians with Bonferroni correction).

In summary, we found that mice vary their search strategy and orient towards the spot as they approach it. Mice also slowed down as they approach the spot. Together, these behavioral changes potentially represent a speed-accuracy trade-off during the final stage of navigation towards an odor object, roughly within ~ 10-45cm.

Casting increases near the odor spot and is modulated by velocity

Casting is seen in diverse odor navigation circumstances ranging from plume navigation by moths to trail tracking by dogs; thus, mice may also cast during the open field odor-based spot-finding task. To measure casting amplitude, we calculated the $\log_{10}$ of the absolute value of the angular velocity of the nose divided by the linear velocity of the nose (Figure 1C; and see Methods). This is an appropriate measure for unsigned path curvature with units of (m^{-1}). We found that curvature increased as mice approached the odor source (ANOVA; p=2.2E-117, F=23.4, df=28) with an interaction between distance and successful versus unsuccessful trials (two-way ANOVA; p=0.0041, F=1.85, df=28).

We used a stepwise Generalized Linear Model (GLM) to determine the relative effect of velocity and distance on the curvature measure of casting. The first term to include in the stepwise GLM was velocity ($p<1E-100$, $F=9636$, Deviance=1500) and the second was distance ($p=7.1E-41$, $F=1481$, Deviance=1481). No nonlinear terms were added to the model.

As curvature explicitly depended on inverse nose velocity (see Methods and results from stepwise GLM), we computed the angle between the head and body centerline as an alternate measure of casting (Figure S3B). Using this alternate measure of nose deflection, we again found that casting increases as mice approach the odor source (ANOVA; $p=2.18E-56$, $F=12.82$, df=28), with an interaction between distance and successful versus unsuccessful trials (two-way ANOVA; $p=0.02$, $F=1.61$, df=28).

To assess whether animals began using non-odor cues to navigate towards the odor spots on later trials, we performed one-way ANOVAs on curvature versus binned trial number (N=6). We found an effect of session on curvature (ANOVA; $p=1.42E-11$, $F=12.34$, df=5), suggesting that after 60-70 trials, a shift in strategy occurred which led to systematically less casting. Further analysis revealed that this effect was consistent with systematically increased nose velocity on later trials (ANOVA; $p=9.16E-7$, $F=7.36$, df=5).

We also examined casting amplitude as a function of approach vector. To compute approach vectors, the angle of the nose with respect to the body was taken and positions were centered with respect to the spot, then binned every 2.3cm. The length of the vector was then normalized by the standard deviation of the angles at that point. The vector colormap indicates the $\log_{10}(|dphi|/nV)$ at that point. Note that on most trials mice approached the spot from the northeast direction (the 'downwind' direction, see Figure 1D). It was in this direction, at points closest to the source, where casting increased (Figure 4B).

Overall, we found that casting amplitude of mice increases at distances close to the spot, suggesting that it may play a role in the successful navigation to a discrete odor object by mice. This change in casting is potentially correlated with velocity, which also decreases significantly during the approach to the spot.

A concentration-sensitive model (CSM) was developed to capture key aspects of mouse behavior discovered on the spot-finding task.

The core of the CSM model is the temporal comparison of sniff-to-sniff concentration. At each discrete "sniff," it samples the odor at the position of its nose and compares the current odor concentration with the previously sampled concentration. Part of the algorithm averages across the two nares (Eq n8) while one component (binaral component) compares the difference between nares (right-most term in Eq n5). A typical simulated nose trajectory showing a successful capture displays inter-sniff differences in odor concentration in arbitrary units (Figure 5C). The CSM model used here had parameters: Δt=0.1s, ℓ=5 cm, v_{max}=25cm/s, k=0.5 concentration units, τ=0.1 s, σ_{min}=0.2 radians, σ_{max}=0.3 radians, and $k_{binaral}$=200 The value of τ chosen gave a good balance of sharp turning nose trajectories with smooth nose trajectories. Values an order of magnitude lower resulted in tight spirals of the nose, while values an order of magnitude higher resulted in loss of maneuverability of the model. v_{max} was chosen as it was the approximate average velocity of mice. Because simulated odor concentrations were scaled to a maximum of one, *k*=0.5 was chosen as the half-maximal value for behavioral response. Changing *k* could be used to 'tune' the model's performance without qualitatively affecting its trajectories. Values of σ_{min}, σ_{max}, and $k_{binaral}$ were chosen so that the model's nose curvature remained qualitatively "mouselike" in character. *I.e.*, the model trajectories did not appear overly tortuous or linear when compared by eye to the mouse trajectories.

To model the observed decrease in velocity close to the odor source, we implemented a concentration-dependent velocity term (Eq n9). In this term, the maximum velocity, v_{max} decreases with increasing concentration according to a sigmoidal function. This function was chosen as it was roughly linear in the center of the concentration range and saturated at high concentrations. To model the increase in curvature with approach to the spot, a concentration-dependent widening of the normal distribution was implemented (Eq n7). These equations were linked by a common parameter *k* that controlled their rates of change as a function of concentration.

As a control, we created a Correlated Random Walk (CRW) model that turned independently of concentration (Eq n14), aligning its heading with its nose 50% of the time and away from its nose 50% of the time, resulting in left and right turns in equal proportion. Models using odor cues to navigate should outperform the CRW.

552

553 *CSM simulations have similar general properties to mice.*

554

555 From our data, we formulated a hypothesis that mice are detecting concentration gradients in order
556 to navigate to the target. While some prior work has suggested that animals can navigate to
557 sources without concentration gradients (Balkovsky & Shraiman, 2002; Vergassola et al., 2007),
558 which may be necessary in highly turbulent environments, odor concentration gradients will
559 develop over time through convection-diffusion and are a likely candidate for rapid olfactory
560 navigation to targets under conditions of low turbulence. We refined our hypothesis to suggest that
561 mice are 1) moving rapidly where the slope of the gradient is low and detecting changes at different
562 physical locations (a versus b); versus, 2) moving slowly where the slope of the gradient is high
563 and detecting changes by sweeping their heads back and forth (A versus B), which we interpret as
564 casting (Figure 5A).

565

566 Initially, we had used a simple stimulus model of multiplicative random noise added to a smooth
567 gradient. However, after examining the fluctuations of concentration near the table on a PID, we
568 decided to implement a more complex odor stimulus model. This included 1) generation of a
569 smooth concentration gradient; 2) addition of multiplicative noise which increased near the source;
570 3) setting pixels equal to zero at a proportion dictated by an intermittency fit such that the farther
571 away from the source the higher proportion of zeros; and, 4) the smoothing of the resulting
572 stimulus by a two-dimensional local Gaussian filter (Figure 5B).

573

574 The CSM model with 4-step stimulus generation generally resembled mouse behavior (Figure 5C).
575 Here, concentration difference between consecutive samples is plotted so that the turning away
576 from high-to-low and turning towards low-to-high concentrations is visible. The simulated odor spot
577 is indicated by the red circle.

578

579 Spots positions for the CSM and CRW were taken from the mouse data, with spots less than 10cm
580 from the edges being removed. The success rate of the CSM was 94%, significantly greater than
581 the 19% for CRW controls (Figure 5D; Welch's t-test; $p=2.16E-22$, t-stat=59.45, df=17). The CSM
582 therefore successfully used information about concentration to navigate within 1.5cm of the odor
583 source.

584

585 The nose displacement over initial distance ratio for the CSM (~5.6x) was significantly less than the
586 CRW (~13x) (Figure 5E; Welch's t-test; p=3.5E-11, t-stat=-34-41, df=9), indicating that the CSM
587 found the odor spots more effectively than the CRW. The survival function of CSM minimum
588 distance to the spot was shifted to left and up compared to the CRW control (Figure 5F). The
589 probability of finding the spot measure for the CSM was also consistently higher than the CRW
590 control (Figure 5G).
591
592 *Examining the structure of CSM trajectories suggests that they approximate mouse behavior.*
593
594 The orientation relative to the spot for the CSM was qualitatively similar to mice (Figure 6A,
595 compare with Figure 3D). The CSM occupancy increased with respect to the CRW occupancy as
596 agents approached the spot (Figure 6B; two-sample Kolmogorov-Smirnov test; p<1E-10 at
597 <26cm). This was similar to the occupancy observed in mice on successful trials (Figure 3B).
598 Mean nose velocity of the CSM decreased as agents approached the spot (Figure 6C), as
599 expected, given eq n9. On successful trials, the CSM explored *less* than it did on unsuccessful
600 trials (Figure 6D). This contrasts with the behavior observed in mice (Figure 3A), suggesting that
601 there are unexplored differences between the CSM and mice. CSM casting increased as agents
602 approach the spot (Figure 6E), as expected, given eq n7. This approximates the effect observed in
603 mice (Figure 4A).
604
605 *Simulations allow separation of component strategies for odor-driven navigation.*
606
607 Simulations allowed for further dissection of the odor-driven factors that impact behavior and
608 successful odor source localization such as decrease in velocity close to the source, increase in
609 casting close to the source, and binaral sniffing. We created reduced CSMs to examine the relative
610 contributions of three hypothesized behavioral components: binaral-sniffing, concentration-
611 dependent velocity, and concentration-dependent casting amplitude. These model variants are
612 denoted (-V) for the model lacking concentration-dependent velocity, (-B) for the model lacking
613 binaral olfaction, (-C) for the model lacking concentration-dependent casting, (-VC), (-VB), (-SC) for
614 models lacking multiple components, and (-VBC) for the model lacking all three components. While
615 all reduced model variants outperformed CRW controls (Figure 7A), removal of any of these
616 behavioral components decreased model success. The removal of concentration-dependent
617 velocity led to the largest change in success rate (-V, Δ30%), followed by concentration-dependent

618 casting amplitude (-C, Δ8%), and binaral-sniffing (-B, Δ3%). The change in success rate was
619 significant for removal of concentration-dependent velocity (Welch's t-test; p<1E-100, t-stat=169,
620 df=1472), concentration-dependent casting (Welch's t-test; p<1E-100, t-stat=58.3, df=1759), and
621 binaral sniffing (Welch's t-test, p=2.65E-100, t-stat=22.6, df=1927). The effect size depended on
622 the number of bootstrapped samples (out of 100,000) and groups in each sample. For this
623 analysis, we chose 1000 groups with 10,000 samples in each group, selected without replacement.
624
625 These behavioral components of olfactory search are synergistic; simultaneous removal of two or
626 more of them leads to a greater reduction in success rate than removal of individual components.
627 Model variant (-VC), in which both velocity decrease and casting increase are removed, resulted in
628 a significant Δ12% change in model success relative to (-V) alone (Welch's t-test; p<1E-100, t-
629 stat=-55.9, df=1997). All groups performed significantly better than the CRW Control, even with all
630 three additional components of the model removed (-VBC; Welch's t-test; p<1E-100, t-stat=67.08,
631 df=1997). This is logical since (-VBC) still makes decisions based on inter-sniff concentration
632 differences, while the CRW Control makes random decisions.
633
634 Significance of model parameters was also established by shuffling 12 parameters of the model
635 50k times, and comparing the effect of each parameter using a logistic regression (Table S2). We
636 also included two dependent variables from the model trajectories that we thought might impact
637 success rate, the mean casting ($\log_{10}$(|dPhi|/nV) within 30cm, and the mean nose velocity within
638 30cm. Note that for this analysis, we split *k* into separate parameters for casting ($k = k_c$in eq n7)
639 and velocity ($k = k_v$in eq n9). Likewise, we labeled and varied the power parameters (n_c = 1 in eq
640 n7) and (n_v = 4 in eq n9) from 0 - 5. We also added a coefficient in front of the *tanh* binaral term in
641 eq n5 ($k_{binaral2}$), and where $k_{binaral}$ in eq n5 is relabeled as $k_{binaral1}$. All parameters and both
642 dependent variables significantly impacted success rate, except for the parameters τ, σ_{min}, and k_c.
643
644 To more rigorously test the effects of different levels of noise, the noise level k_n in eq n11 (also see
645 step 2 in Figure 5B) was varied from 0 to 1 and the Gaussian smoothing (4mm in reported CSM
646 variant; step 4 in Figure 5B) was varied from 0mm to 10mm. Success rate rapidly dropped off as
647 k_n approached 1 or smoothing approached 0mm (Figure 7B).
648
649 To more rigorously test the effects of the 2-parameter binaral term, we re-ran the 6 reduced model
650 variants 100,000 times each with a coefficient of $k_{binaral2}$ =3 in front of the *tanh* term in eq n5. Again,

651 we chose 1000 groups with 10,000 samples in each group, selected without replacement. This
652 resulted in smaller effects of removing (-V) and (-C), but a larger effect of removing (-B), suggesting
653 that strong binaral-sniffing may be able to compensate for removal of variable velocity and casting
654 (Figure 7C).
655
656 In summary, reduced models revealed that individual components of the overall strategy worked
657 together to maximize task performance, with concentration-dependent velocity and binaral-sniffing
658 having the greatest impact on successful task performance.
659
660
661 **DISCUSSION**
662 Here, we described the navigation strategies of mice during an open field odor-based spot-finding
663 task. Over the course of 7-10 trials, mice could be trained to perform this task on a 45" x 36" open
664 field arena. Performance of mice exceeded that of shuffled controls, indicating that mice were
665 using odor cues to localize the odor target. Olfactory-guided behavior changed as a function of
666 distance; specifically, 1) nose velocity decreased close to the source, 2) casting increased close to
667 the source, and, 3) occupancy increased close to the source. Mice demonstrate reliable spot-
668 finding within 10-45cm of the odor source. The Concentration Sensitive Model (CSM) was built to
669 capture these observations by incorporating concentration-dependent velocity and casting terms,
670 as well as a postulated binaral comparison term. Removing components of the CSM demonstrated
671 that each had a significant impact on performance.
672
673 *There is a potential speed-accuracy trade-off in search strategy close to the odor spot.*
674
675 As mice approach an odor source, they slow down and increase their exploration time in a smaller
676 annulus around the spot. This is similar to observations in fruit flies following a plume upwind to an
677 odor source (Budick & Dickinson, 2006). We suggest this phenomenon may be a type of speed-
678 accuracy trade-off (Heitz, 2014) in olfactory search behavior. Specifically, when concentration
679 reaches some perceptual threshold, mice may "switch" into a local search strategy designed to
680 increase accuracy at the expense of speed to target. In this local search strategy, the mouse
681 spends more time in regions of high concentration where it is more likely to hit its target. In
682 agreement with this hypothesis, elimination of concentration-dependent velocity decrease led to
683 less success in reduced models (Figure 7A). An alternative explanation is that as the mouse

684 approaches the odor source, it may reduce its running speed to avoid ‘overshooting’ the odor
685 source.
686
687 *Binaral-sniffing facilitates search near the odor source.*
688
689 Use of binaral-cues for navigation has been observed in moles (Catania, 2013), snakes (Schwenk,
690 1994), and insects (Martin, 1965; Steck et al., 2010) suggesting it may be an evolutionarily
691 conserved strategy. In mammals, neurons in the anterior olfactory nucleus may play a key role in
692 integration of bilateral stimuli that are key to binaral-sniffing (Kikuta et al., 2010) as this is one of
693 the earliest locations in which information from both left and right naris can be integrated. We
694 suggest that binaral-sniffing cues may play a pivotal role in fine discrimination of odor identity
695 (Uchida & Mainen, 2003), as opposed to gross determination of odor source localization in space.
696 Once a trail’s direction, or the rough direction to a spot is determined, binaral-sniffing cues may be
697 useful for determining the direction to cast in order to continue following the direction of the trail
698 (Khan et al., 2012), or steer towards the odor spot. Binaral-sniffing allowed the CSM to
699 preferentially cast in the direction of the odor source only when the odor gradient was large (i.e.,
700 near the source). Removal of binaral-sniffing led to a statistically significant decrease in CSM
701 success (Figure 7C), an observation compatible with the model developed by Catania, 2013,
702 where binaral-sniffing becomes a relevant strategy on steep concentration gradients. Depending
703 on the strength of the $k_{binaral}$ term (Eq n5), binaral-sniffing may help bias increased lateral search
704 towards the direction of the source, allowing the nose to be “pulled” toward the source in relatively
705 smooth arc-like trajectories.
706
707 Future research should examine if the physical distance between nostrils is correlated with the
708 ‘effective’ nares separation of air drawn into the nasal cavity, or if the effective nares separation is
709 determined by physical parameters such as inhalation volume, flux, and gradient. For example,
710 inhalation in rats is largely from the lateral direction, rather than the front of the animal (Wilson &
711 Sullivan, 1999). Pressure differences generated during sniffing inhalation at different magnitudes
712 and frequencies (slow deep breath versus rapid sniffing) may also draw in relatively different
713 concentrations of molecules from different distances away from the nares.
714
715 *Odor source localization may rely on cognitive mapping*
716

717 Navigation to an odor source with serial-sniffing is probably intimately tied to navigation through
718 space using the cognitive map (Jacobs, 2012). Specifically, the distance traveled between the first
719 to the second sniff in the concentration comparison helps determine an updated heading towards
720 the source or along the trail. In support of this view, hippocampal place cells may change their
721 firing patterns (called remapping) to match the relocation of an orienting odor source in a circular
722 arena (Zhang & Manahan-Vaughan, 2015). Thus, serial-sniffing is potentially more relevant to
723 gross odor localization than binaral-sniffing. For example, to determine trail direction using binaral-
724 sniffing most efficiently, an animal would have to be oriented roughly perpendicular to the trail so
725 that its nares are sensing maximally different concentrations. In contrast, studies with dogs
726 repeatedly find that serial-sniffing of 2-5 footprints is required to determine a trail's direction
727 (Hepper & Wells, 2005; Thesen et al., 1993). Similarly, initial odor source seeking may utilize
728 serial-sniffing to quickly map larger spatial areas, including eliminating subspaces where no odor is
729 detected (Vergassola et al., 2007).
730
731 *Casting is related to olfactory-guided navigation to a discrete, static odor source.*
732
733 Casting has been observed at frequencies of ~4 Hz in moths flying upwind during pheromone-
734 tracking (Charlton et al., 1993), and similar head-scanning behaviors have been observed in
735 *Drosophila* larvae, rats, moles, and humans (Baker et al., 2018). In moths, casting has been
736 reported to occur *outside* of an odor plume when a moth is attempting to re-acquire the odor
737 (Kennedy, 1983) and is characterized by loop-like flight trajectories (Kuenen & Carde, 1994). In
738 contrast, here we find that mouse casting amplitude increases during approach to the odor source.
739 The moth data suggest that casting increases whenever there are intermittent gaps in the odor
740 signal, as they cast to re-acquire the odor plume. If this were true for mice performing this task, we
741 would expect casting to be higher farther away from the odor source where the signal is sparse.
742 The nature of this task, where mice seek a discrete odor object on a near-bed surface rather than
743 an odor plume in the air, may explain these differences in behavior. While we did not find that
744 addition of concentration-dependent casting improves performance (Figure 5B), we did not prove
745 that this was true for all parameter sets in the CSM model. Therefore, a set of untested parameters
746 may explain the lack of improvement with addition of concentration-dependent casting.
747
748 *Complexities to address in future studies include decision-rules and individual variability in strategy*
749 *utilization.*

750

751 Our data suggest that mice may use multiple search strategies during an open field odor-based
752 spot-finding task depending on their distance from the source. We speculate that the relative
753 contribution of strategies may also be variable between individuals, as has been observed during
754 fruit fly navigation during odor presentation (Tao et al., 2019). This may mean a specific
755 instantiation of our model (with one set of parameters) captures behavior for one individual mouse,
756 but fails to capture behavior for some other subset of mice. For example, we found that the *k*
757 parameter could be used to 'tune' aspects of the model's trajectories which may better fit the data
758 for a subpopulation of mice. A much larger cohort of animals than was used here would be
759 necessary to evaluate this idea; however, the general principle is that similar-looking ethologically-
760 relevant behavior can emerge from different model permutations.
761

762 A limitation of the current model is that it incorporates an 'all or nothing' decision at each sniff. It
763 may be more appropriate to use a probabilistic decision rule to combine binaral- and serial-sniffing
764 into a unified output. Also, a model where pausing emerges during epochs of uncertainty in
765 sampling of the odor concentration gradient may be advantageous. Additionally, the model is
766 currently limited to detection of one odorant—it would be useful to distinguish different features of
767 diverse odorants. Finally, stimulus models with 'zeros' distributed throughout the simulated odor
768 landscape produced high failure rates. Developing a model that is robust to this type of
769 intermittency would be a logical next step.
770

771 We show that the CSM is capable of using serial concentration sampling of gradients to locate
772 odors, even when the odor landscape has many local minima and maxima surrounding the odor
773 source (e.g., Figure 5B, step 4). While the CSM is capable of finding the odor source when the
774 odor is consistently above threshold, it does not attempt to capture mouse behavior in the
775 environmental regime where the odor concentration is below the animal's detection threshold.
776 Rather than attempting to model mouse behavior in this subthreshold condition, the CSM engages
777 in a correlated random walk that may bring it in contact with suprathreshold odor concentrations.
778 The mouse may be engaging in more complex navigation behavior in this dilute regime, including
779 mapping of the odor environment. Models that attempt to navigate complex odor landscapes
780 without gradient ascent have their own drawbacks. The model of Balkovsky and Shairaman, 2002
781 requires an additional wind cue - anemotaxis - to function properly. The model of Vergasolla, *et* al,

2007 builds a cognitive map of odor source location likelihood; it utilizes both sparse odor detection events and frequent subthreshold observations to update its map of source location likelihood.

In summary, we discover that mice vary their search strategy, including casting, during active navigation toward a discrete odor object, modulating features of behavior as a function of distance from the target. A concentration-sensitive model successfully reproduces mouse behavior, while allowing for the analysis of the relative contributions of binaral-sniffing, concentration-dependent velocity, and concentration-dependent casting amplitude. Future work is needed to experimentally dissect how these variables impact mouse navigation and whether additional parameters are important in successful navigation to a static odor source.

ACKNOWLEDGEMENTS

We thank Gregory LaRocca for technical help, and members of the Urban laboratory as well as Yu Chen, Robert Kass, Nour Riman, Erin Connor, and John Crimaldi for helpful discussions. We thank Kathy Nagel and Jonathan Victor for helpful comments on an earlier draft of the manuscript. A special thanks to Peter Jones for designing and building the behavior table used in this experiment. Thanks to Chris D. Rand from Aurora Scientific for technical help with the PID.

COMPETING INTERESTS

The authors declare no competing financial interests.

FUNDING

This work was supported by the National Science Foundation [1555862 to N.N.U., 1555916 to B.E.]; the National Institutes of Health, National Institute on Deafness and Other Communication Disorders [F30DC015161 to A.L.], and the Pennsylvania Department of Health's Commonwealth Universal Research Enhancement Program [N.N.U.].

FIGURE CAPTIONS

Figure 1. Experimental setup and methods. A) The behavioral arena is a 45" x 36" table made from three layers of plexiglass, with an infrared (IR) camera placed underneath to view the mice from below. Odor spots were placed pseudo randomly on the table by the experimenter before starting the trial, either unbaited or baited with a food reward. (Adapted with permission from Jones

815 and Urban, 2018.) **B)** The pseudo random odor spot distribution for all trials (N=853). **C)** An
816 example trajectory where the mouse finds the odor spot, showing nose tracking with the casting
817 measure (unsigned curvature) on the color axis. The mouse is placed on the right side of the table
818 and begins to hone in on the odor spot (red circle). The casting measure clearly indicates points of
819 high curvature (yellow) from points of high linearity (blue). **D)** Anemometer measurements at 9
820 positions across the behavioral arena. Average wind speed in the <x> and <y> direction are
821 indicated by the text at each point, with estimated wind velocity vectors indicated by the green
822 arrows. **E)** Photoionization Detector (PID) readings from 0.5cm to 15cm away from an odor source
823 placed at the center of the table (gold star in Figure 1D). Measurements were taken to the right of
824 the star, in the 'downwind' direction. **F)** PID analysis suggests that mean signal variance, mean
825 signal amplitude, and intermittency decrease starting at about 2.5cm from the source out to about
826 15cm.
827
828 **Figure 2. Mice and the CSM efficiently locate the odor source. A)** The survival function shows
829 the fraction of closest distances to the spot as a function of distance from the spot. At about 1.5cm
830 away from the spot, the closest distance starts to drop off for mice, suggesting this would be a
831 good threshold distance for counting a trial as successful. In comparison, there is no sharp
832 distinction in the shuffled control data. Instead, shuffled minimum distances tend to increase
833 smoothly as a function of increasing distance. At about 30cm away from the odor spot, the
834 minimum distances are indistinguishable between mice and shuffled controls. **B)** Mice are more
835 successful at finding the odor spots than shuffled controls, suggesting that they are using odor
836 cues to guide their search. **C)** The time to spot is divided by the initial distance to the spot, and
837 mice find the spot more quickly than shuffled controls. **D)** The nose displacement was divided by
838 the initial distance to the spot, and the relative distance traveled by the nose of mice is less than
839 that of the shuffled controls. **E)** The number of samples in 100 concentric rings around the spot
840 were counted up. The number of samples in each ring on successful trials was divided by the total
841 number of samples to give a measure of probability of finding the spot as a function of distance.
842 This measure decreased roughly linearly for mice but highly nonlinearly for shuffled controls. This
843 suggests mice are efficiently navigating toward the spot.
844
845 **Figure 3. Mouse behavior varies systematically as mice approach the odor source. A)** The
846 center of the arena was broken up into bins of different area and the percentage of those bins
847 visited by mice was counted up and plotted versus the bin area. In general, this 'exploration

848 percentage' increased with increasing bin size, while successful trials entailed a higher exploration
849 percentage than unsuccessful trials. **B)** The number of samples in 100 concentric rings around the
850 spot was tallied, and normalized by both the total number of samples in a given trial and the area of
851 the ring. This gave a measure of occupancy with units of $\%/cm^2$. As mice approach the spot on
852 successful trials, their occupancy increases. In contrast, the occupancy on unsuccessful trials
853 remains flat as a function of distance. **C)** Mean nose velocity decreases as mice approach the
854 spot on successful trials. In contrast, mean nose velocity remains flat as a function of distance on
855 unsuccessful trials. **D)** The orientation of the mouse relative to the odor spot was computed and
856 normalized to 100% at each distance from the spot. For this measure, orientation of 0° indicates
857 that the mouse's nose is pointing directly at the odor spot and an orientation of 180° means that it's
858 nose is pointing away from the odor spot. Orientation tends to converge at 0° as mice approach
859 the odor spot. **E)** Diagram demonstrating the computation of orientation relative to the spot. The
860 angle β between the body and spot (red circle) is subtracted from the angle α between the nose
861 and the body.
862
863 **Figure 4. Analysis of casting amplitude using curvature. A)** Unsigned curvature of the nose
864 was computed as a measure of casting amplitude (see Methods) and averaged across successful
865 trials (red line=mean±s.e.m.). Casting increased as mice approached the odor spot (ANOVA;
866 p=1.21E-64, F=42, df=8), and was significantly higher on successful trials within ~12 cm compared
867 to unsuccessful trials (Welch's t-test, p=7.2E-5, t-stat=-4.26, df=61, Bonferroni correction). **B)** The
868 approach vector for successful trials are the vector components of the circular mean of the nose-to-
869 body orientation after centering position data at the odor spots. Vectors are normalized by the
870 circular standard deviation. Color indicates the curvature measure for casting at that point. Most
871 trajectories approach the spot from the northeast.
872
873 **Figure 5. Development of concentration-sensitive model. A)** Our general hypothesis in
874 constructing the model was that lower concentration differences (ΔC_{ab}) far from the source would
875 be detectable by gross movement of the body (right panel). In contrast, higher concentration
876 differences (ΔC_{AB}) would be detectable by fine movement of the head (left panel). In this
877 illustration, the wavy green line represents the concentration of an odorant. The blue shading
878 indicates averaging concentration over an inhalation. The dashed lines indicate the mean
879 concentration for each sniff. **B)** The odor concentration profile was constructed in four steps: 1) A
880 smooth concentration gradient was computed; 2) multiplicative random noise was added to the

881 gradient; 3) 'Intermittency' was modeled by setting a proportion of pixels equal to zero. This
882 proportion increased with distance from the source. Finally, 4) Gaussian smoothing was
883 implemented to simulate averaging of the signal over a sniff. **C)** An example trajectory from the
884 concentration-sensitive model (CSM) that successfully found the odor spot (red circle).
885 Concentration difference (A.U.) is indicated. **D)** The success rate of the CSM was above 75%,
886 while the CRW control model had a success rate of below 25%. **E)** The nose displacement divided
887 by the initial distance to the spot was lower for the CSM than for the CRW control, indicating more
888 direct travel to the odor spot using concentration to guide the model. **F)** The survival function of
889 approach distances shows that nearly all CSM trajectories approach within 30cm of the source,
890 while CRW control trajectories are more spread out across the entire table. **G)** The probability of
891 finding the odor spot was computed for the models as in Figure 2E. With this measure, the CSM
892 was more successful at finding odor spots at all distances from the spot compared to CRW
893 controls.
894
895 **Figure 6. Detailed analysis of CSM trajectories. A)** The orientation of the CSM model relative
896 to the odor spot resembled that of mice (compare Figure 3D). **B)** The occupancy of the CSM
897 resembled that of mice (magenta line; compare red line Figure 3B), and significantly diverged from
898 the CRW control (gray line) at around 20cm from the odor spot. **C)** The mean nose velocity of the
899 CSM (magenta line) decreased as the model approached the odor spot, consistent with what was
900 observed with mice (compare red line Figure 3C). The nose velocity of the CSM was different from
901 the CRW control (gray line). **D)** In contrast to mice, successful trials of the CSM (magenta line)
902 showed *less* exploration than unsuccessful trials (gray line) (compare red line to blue line in Figure
903 3A). **E)** Casting increased as the CSM approached the spot (magenta line) consistent with
904 observations in mice (compare red line Figure 4A). Casting in the CSM increased with respect to
905 the CRW control (gray line) at a distance of 7cm.
906
907 **Figure 7. Analysis of reduced models and parameter sweeps. A)** The full model (CSM)
908 included three components: 1) a concentration-dependent velocity term (V), 2) a concentration-
909 dependent casting term (C); 3) a binaral-olfaction term (S). Removal of any of these components
910 (-V), (-B), or (-C) may, in principle, reduce model performance. Removal of concentration-
911 dependent velocity (-V) had the largest effect on performance. Removal of concentration-
912 dependent casting (-C) had a smaller effect on performance. Removal of binaral-olfaction (-B) had
913 the smallest effect on performance. Removal of both concentration-dependent velocity and casting

(-VC) had a multiplicative effect on performance. Removal of all three components (-VBC) was still significantly better than CRW controls. **B)** Comparison of noise effects on CSM success rate shows that the CSM model is robust for a wide array of different noise conditions. **C)** Because (-B) had the smallest effect on performance, we wished to investigate its role further. We added a coefficient in front of the hyperbolic tangent term in eq n5 and set it equal to 3. With this additional term, success rate reduction from removing the binaral term increased. However, success reduction from removing (-V) or (-C) terms decreased. This suggests that binaral sniffing can compensate somewhat for lack of velocity or casting changes.

SUPPLEMENTAL CAPTIONS

Figure S1. Example Traces. Successful trials (left and center panels) have the time to spot indicated by the text. The relative time of each position sample is indicated by the color. Unsuccessful trials (right panel) have the total trial time indicated by the text. Color represents the relative time of each position sample. Spot positions are indicated by red circles.

Figure S2. Detailed model geometry. A) Model specification of the body position (x,y), and the body angle θ superimposed on a diagram of the mouse. The nose position (x_n,y_n) is the mean position between the left and right nares. **B)** Nose angle ϕ (gray dashed line) is the angle between θ and nose position. Nose angle ϕ is constrained by a maximum angle ϕ_{max} . The head-body length ℓ is the distance between the body position and the nose position. Nose position is sub-divided into two nostrils (left indicated by red, right indicated by green), separated by a distance d_{nares}. The angle from the center of the nose to the edge of the nostril is γ. **C)** The distribution of mouse nose deflection angles ϕ (blue bars) is approximately Gaussian (dashed red line; a*exp(-((x-b)/c)^2); a=0.04, b=0.06, c=1.92).

Figure S3. Additional Casting Analyses. A) Curvature as measured by $\log_{10}$(|dPhi|/nV) depends on nose velocity. The colormap indicates the percentage of samples in each bin. **B)** Averaged across successful trials, nose deflection angle ϕ increases as the distance to the spot decreases (line=mean±s.e.m; ANOVA; p=2.18E-56, F=12.82, df=28).

Table S1. Logistic regression analysis on spot-finding success in mice. Significant variables in bold.

Table S2. Logistic regression analysis of CSM parameters on spot-finding success. Significant parameters are in bold.

ABBREVIATIONS

CSM – concentration-sensitive model

CRW – correlated random walk

OU – Ornstein-Uhlenbeck

Δt – change in time (s)

ℓ – nose-to-body length parameter (cm)

v_{max} – maximum velocity parameter (cm/s)

k – concentration-dependent parameter

σ_{min} – concentration-dependent parameter

σ_{max} – concentration-dependent parameter

$k_{binaral}$ – binaral-olfaction parameter

d_{nares} – inter-nostril parameter (cm)

ANOVA – Analysis Of VAriance

LED – light emitting diode

|dPhi|/nV – curvature

x' – derivative (of x)

x_n – nose coordinate

θ – heading of model body (degrees)

φ – heading of model nose relative to body (degrees)

C_t – concentration magnitude (A.U.)

η_t – multiplicative uniform noise

(-C) – CSM model without concentration-dependent casting, $\sigma = \sigma_{min}$

(-B) – CSM model without binaral-sniffing component, $k_{binaral}=0$

(-V) – CSM model without concentration-dependent velocity, $v=v_{max}$

IR – infrared

REFERENCES

Baker, K. L., Dickinson, M., Findley, T. M., Gire, D. H., Louis, M., Suver, M. P., . . . Smear, M. C. (2018). Algorithms for Olfactory Search across Species. *Journal of Neuroscience, 38*(44), 9383-9389. doi:10.1523/JNEUROSCI.1668-18.2018

Balkovsky, E., & Shraiman, B. I. (2002). Olfactory search at high Reynolds number. *Proceedings of the National Academy of Sciences of the United States of America, 99*(20), 12589-12593. doi:10.1073/pnas.192393499

Ben-Shaul, Y. (2017). OptiMouse: a comprehensive open source program for reliable detection and analysis of mouse body and nose positions. *BMC Biol, 15*(1), 41. doi:10.1186/s12915-017-0377-3

Bhattacharyya, U., & Bhalla, U. S. (2015). Robust and Rapid Air-Borne Odor Tracking without Casting. *eNeuro, 2*(6). doi:10.1523/ENEURO.0102-15.2015

Budick, S. A., & Dickinson, M. H. (2006). Free-flight responses of Drosophila melanogaster to attractive odors. *Journal of Experimental Biology, 209*(Pt 15), 3001-3017. doi:10.1242/jeb.02305

Carde, R. T., & Willis, M. A. (2008). Navigational strategies used by insects to find distant, wind-borne sources of odor. *Journal of Chemical Ecology, 34*(7), 854-866. doi:10.1007/s10886-008-9484-5

Catania, K. C. (2013). Stereo and serial sniffing guide navigation to an odour source in a mammal. *Nat Commun, 4*, 1441. doi:10.1038/ncomms2444

Charlton, R. E., Kanno, H., Collins, R. D., & Carde, R. T. (1993). Influence of Pheromone Concentration and Ambient-Temperature on Flight of the Gypsy-Moth, Lymantria-Dispar (L), in a Sustained-Flight Wind-Tunnel. *Physiological Entomology, 18*(4), 349-362.

Connor, E. G., McHugh, M. K., & Crimaldi, J. P. (2018). Quantification of airborne odor plumes using planar laser-induced fluorescence. *Experiments in Fluids, 59*(9). doi:ARTN 13710.1007/s00348-018-2591-3

Draft, R. W., McGill, M. R., Kapoor, V., & Murthy, V. N. (2018). Carpenter ants use diverse antennae sampling strategies to track odor trails. *Journal of Experimental Biology, 221*(22). doi:UNSP jeb18512410.1242/jeb.185124

Duval, L. (2018). BEADS: Baseline Estimation And Denoising with Sparsity, version 1.7.0.1. https://www.mathworks.com/matlabcentral/fileexchange/49974-beads-baseline-estimation-and-denoising-with-sparsity

Gire, D. H., Kapoor, V., Arrighi-Allisan, A., Seminara, A., & Murthy, V. N. (2016). Mice Develop Efficient Strategies for Foraging and Navigation Using Complex Natural Stimuli. *Curr Biol, 26*(10), 1261-1273. doi:10.1016/j.cub.2016.03.040

Hangartner, W. (1969). Structure and variability of the individual odor trail in Solenopsis geminata Fabr. (Hymenoptera Formicidae). *Z. Vgl. Physiol., 62*, 111-120.

Heitz, R. P. (2014). The speed-accuracy tradeoff: methodology, and behavior. *Frontiers in Neuroscience, 8*. doi:ARTN 15010.3389/fnins.2014.00150

Hepper, P. G., & Wells, D. L. (2005). How many footsteps do dogs need to determine the direction of an odour trail? *Chemical Senses, 30*(4), 291-298. doi:10.1093/chemse/bji023

Hills, T. T., Todd, P. M., Lazer, D., Redish, A. D., Couzin, I. D., & Grp, C. S. R. (2015). Exploration versus exploitation in space, mind, and society. *Trends in Cognitive Sciences, 19*(1), 46-54. doi:10.1016/j.tics.2014.10.004

Jacobs, L. F. (2012). From chemotaxis to the cognitive map: The function of olfaction. *Proceedings of the National Academy of Sciences of the United States of America, 109*, 10693-10700. doi:10.1073/pnas.1201880109

Janabi-Sharifi, F., Hayward, V., & Chen, C. S. J. (2000). Discrete-time adaptive windowing for velocity estimation. *Ieee Transactions on Control Systems Technology, 8*(6), 1003-1009. doi:Doi 10.1109/87.880606

Kennedy, J. S. (1983). Zigzagging and Casting as a Programmed Response to Wind-Borne Odor - a Review. *Physiological Entomology, 8*(2), 109-120. doi:DOI 10.1111/j.1365-3032.1983.tb00340.x

Khan, A. G., Sarangi, M., & Bhalla, U. S. (2012). Rats track odour trails accurately using a multi-layered strategy with near-optimal sampling. *Nature Communications, 3*. doi:ARTN 70310.1038/ncomms1712

Kikuta, S., Sato, K., Kashiwadani, H., Tsunoda, K., Yamasoba, T., & Mori, K. (2010). From the Cover: Neurons in the anterior olfactory nucleus pars externa detect right or left localization of odor sources. *Proc Natl Acad Sci U S A, 107*(27), 12363-12368. doi:10.1073/pnas.1003999107

Koehl, M. A., Koseff, J. R., Crimaldi, J. P., McCay, M. G., Cooper, T., Wiley, M. B., & Moore, P. A. (2001). Lobster sniffing: antennule design and hydrodynamic filtering of information in an odor plume. *Science, 294*(5548), 1948-1951. doi:10.1126/science.1063724

Kuenen, L. P. S., & Carde, R. T. (1994). Strategies for Recontacting a Lost Pheromone Plume - Casting and Upwind Flight in the Male Gypsy-Moth. *Physiological Entomology, 19*(1), 15-29. doi:DOI 10.1111/j.1365-3032.1994.tb01069.x

Manurung, A. (2016). Numerical methods for velocity estimation. https://www.mathworks.com/matlabcentral/fileexchange/52381-numerical-methods-for-velocity-estimation

Marsh, D., Kennedy, J. S., & Ludlow, A. R. (1978). An analysis of anemotactic zigzagging flight in male moths stimulated by pheromone. *Physiol. Entomol., 3*, 221-240.

Martin, H. (1965). Osmotropotaxis in Honey-Bee. *Nature, 208*(5005), 59-&. doi:DOI 10.1038/208059a0

Means, L. W., Alexander, S. R., & Oneal, M. F. (1992). Those Cheating Rats - Male and Female Rats Use Odor Trails in a Water-Escape Working Memory Task. *Behavioral and Neural Biology, 58*(2), 144-151. doi:Doi 10.1016/0163-1047(92)90387-J

Papale, A. E., Stott, J. J., Powell, N. J., Regier, P. S., & Redish, A. D. (2012). Interactions between deliberation and delay-discounting in rats. *Cognitive Affective & Behavioral Neuroscience, 12*(3), 513-526. doi:10.3758/s13415-012-0097-7

Pierce-Shimomura, J. T., Morse, T. M., & Lockery, S. R. (1999). The fundamental role of pirouettes in Caenorhabditis elegans chemotaxis. *Journal of Neuroscience, 19*(21), 9557-9569.

Porter, J., Craven, B., Khan, R. M., Chang, S. J., Kang, I., Judkewitz, B., . . . Sobel, N. (2007). Mechanisms of scent-tracking in humans. *Nature Neuroscience, 10*(1), 27-29. doi:10.1038/nn1819

Schwenk, K. (1994). Why snakes have forked tongues. *Science, 263*(5153), 1573-1577. doi:10.1126/science.263.5153.1573

Steck, K., Knaden, M., & Hansson, B. S. (2010). Do desert ants smell the scenery in stereo? *Animal Behaviour, 79*(4), 939-945. doi:10.1016/j.anbehav.2010.01.011

Sutton, R. S., & Barto, A. G. (1998). *Reinforcement learning : an introduction*. Cambridge, Mass.: MIT Press.

Tao, L. Y., Ozarkar, S., Beck, J. M., & Bhandawat, V. (2019). Statistical structure of locomotion and its modulation by odors. *Elife, 8*. doi:ARTN e4123510.7554/eLife.41235

Thesen, A., Steen, J. B., & Doving, K. B. (1993). Behavior of Dogs during Olfactory Tracking. *Journal of Experimental Biology, 180*, 247-251.

Uchida, N., & Mainen, Z. F. (2003). Speed and accuracy of olfactory discrimination in the rat. *Nature Neuroscience, 6*(11), 1224-1229. doi:10.1038/nn1142

Vergassola, M., Villermaux, E., & Shraiman, B. I. (2007). 'Infotaxis' as a strategy for searching without gradients. *Nature, 445*(7126), 406-409. doi:10.1038/nature05464

Vickers, N. J. (2000). Mechanisms of animal navigation in odor plumes. *Biological Bulletin, 198*(2), 203-212. doi:Doi 10.2307/1542524

Wallace, D. G., Gorny, B., & Whishaw, I. Q. (2002). Rats can track odors, other rats, and themselves: implications for the study of spatial behavior. *Behavioural Brain Research, 131*(1-2), 185-192. doi:Pii S0166-4328(01)00384-9Doi 10.1016/S0166-4328(01)00384-9

Wesson, D. W., Donahou, T. N., Johnson, M. O., & Wachowiak, M. (2008). Sniffing behavior of mice during performance in odor-guided tasks. *Chemical Senses, 33*(7), 581-596. doi:10.1093/chemse/bjn029

Willis, M. A., Avondet, J. L., & Finnell, A. S. (2008). Effects of altering flow and odor information on plume tracking behavior in walking cockroaches, Periplaneta americana (L.). *Journal of Experimental Biology, 211*(Pt 14), 2317-2326. doi:10.1242/jeb.016006

Wilson, D. A., & Sullivan, R. M. (1999). Respiratory airflow pattern at the rat's snout and an hypothesis regarding its role in olfaction. *Physiology & Behavior, 66*(1), 41-44. doi:Doi 10.1016/S0031-9384(98)00269-8

Zhang, S. J., & Manahan-Vaughan, D. (2015). Spatial Olfactory Learning Contributes to Place Field Formation in the Hippocampus. *Cerebral Cortex, 25*(2), 423-432. doi:10.1093/cercor/bht239

Zhao, W. Q., Gong, C. X., Ouyang, Z. H., Wang, P. F., Wang, J., Zhou, P. P., . . . Gong, Z. F. (2017). Turns with multiple and single head cast mediate Drosophila larval light avoidance. *Plos One, 12*(7). doi:ARTN e018119310.1371/journal.pone.0181193

FIGURE 1

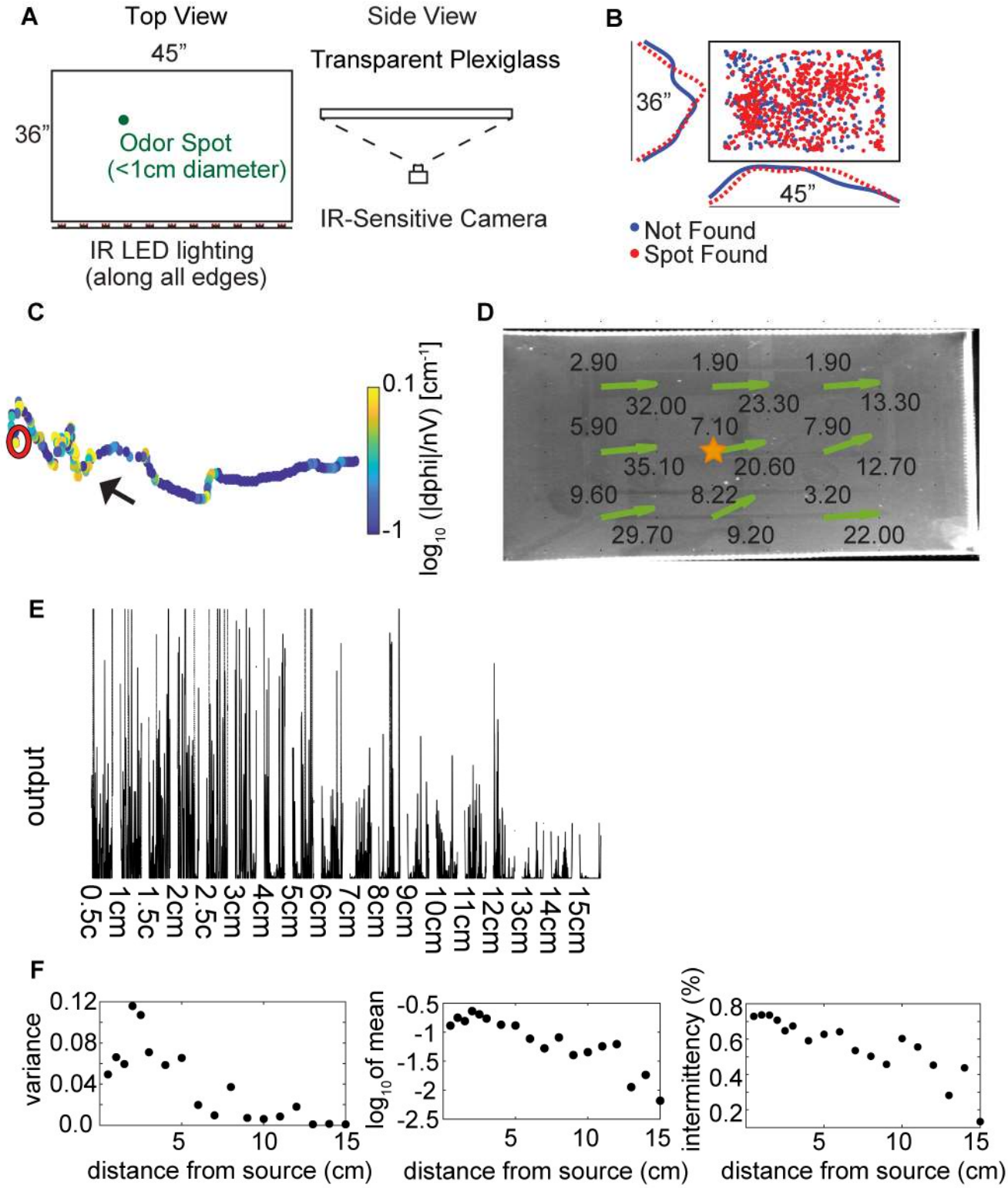
A
Top View
45”
36”
Odor Spot
(<1cm diameter)
IR LED lighting
(along all edges)
Side View
Transparent Plexiglass
IR-Sensitive Camera
B
36”
45”
Not Found
Spot Found
C
0.1
-1
log10 (|dphi|/nV) [cm-1]
D
2.90
1.90
1.90
32.00
23.30
13.30
5.90
7.10
7.90
35.10
20.60
12.70
9.60
8.22
3.20
29.70
9.20
22.00
E
output
0.5c
1cm
1.5c
2cm
2.5c
3cm
4cm
5cm
6cm
7cm
8cm
9cm
10cm
11cm
12cm
13cm
14cm
15cm
F
variance
0.12
0.08
0.04
0.0
5
10
15
distance from source (cm)
log10 of mean
-0.5
-1
-1.5
-2
-2.5
5
10
15
distance from source (cm)
intermittency (%)
0.8
0.6
0.4
0.2
5
10
15
distance from source (cm)

1131
1132
1133
1134
1135 **FIGURE 2**
1136

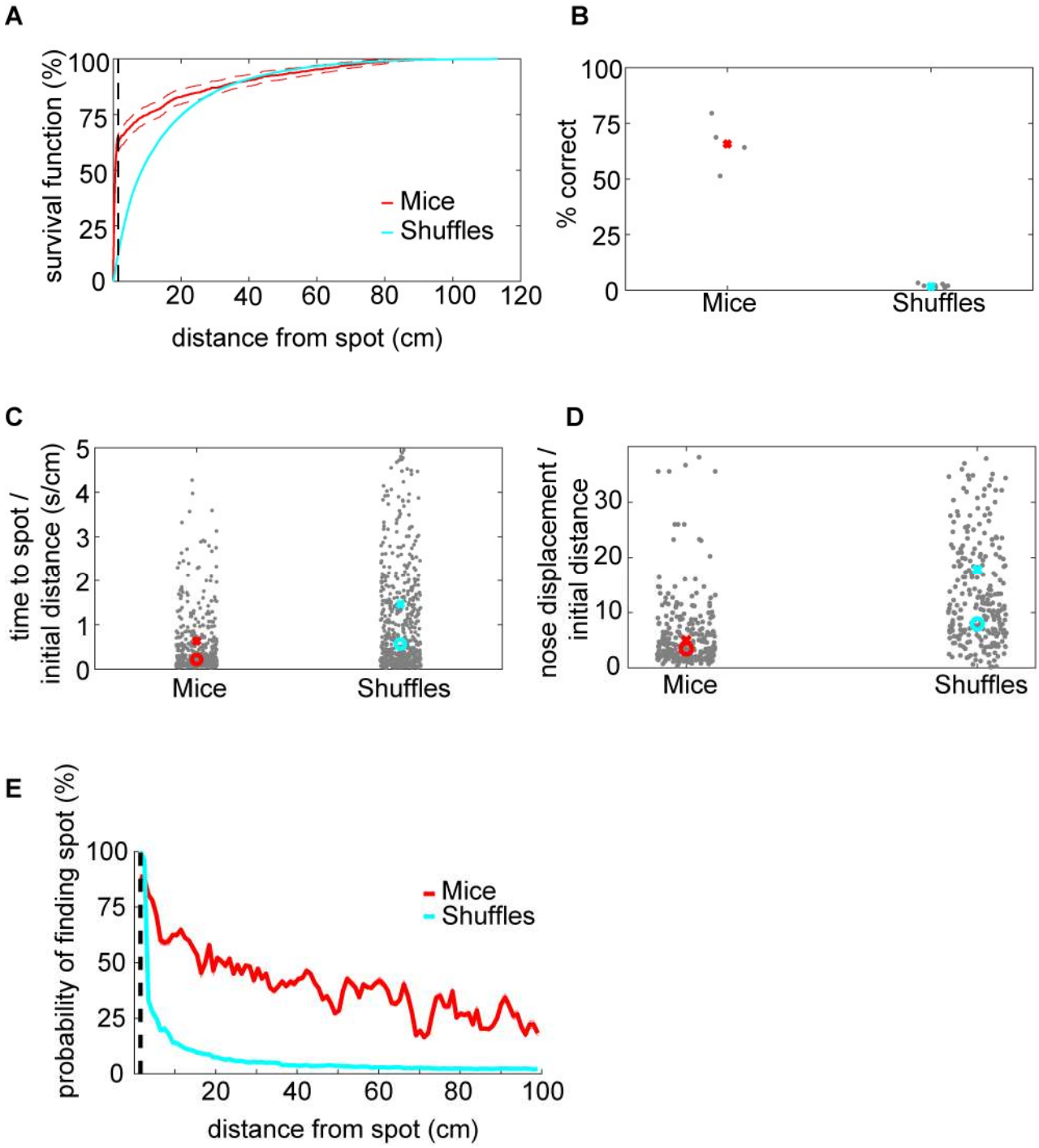

1137
1138
1139

1140

1141

1142

1143 **FIGURE 3**

1144

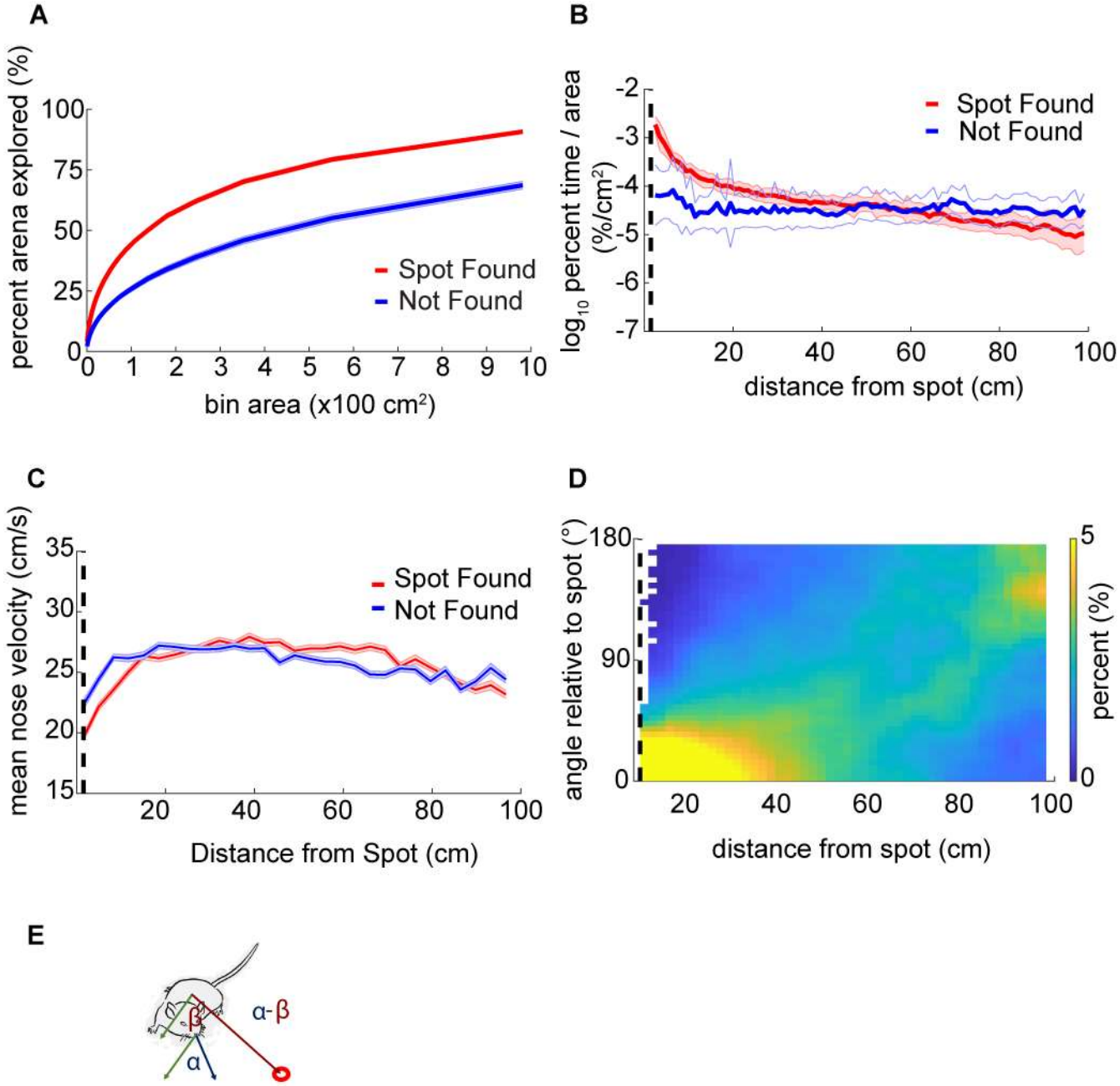

1145

1146

1147

1148

1149

1150

1151

1152 **FIGURE 4**

1153

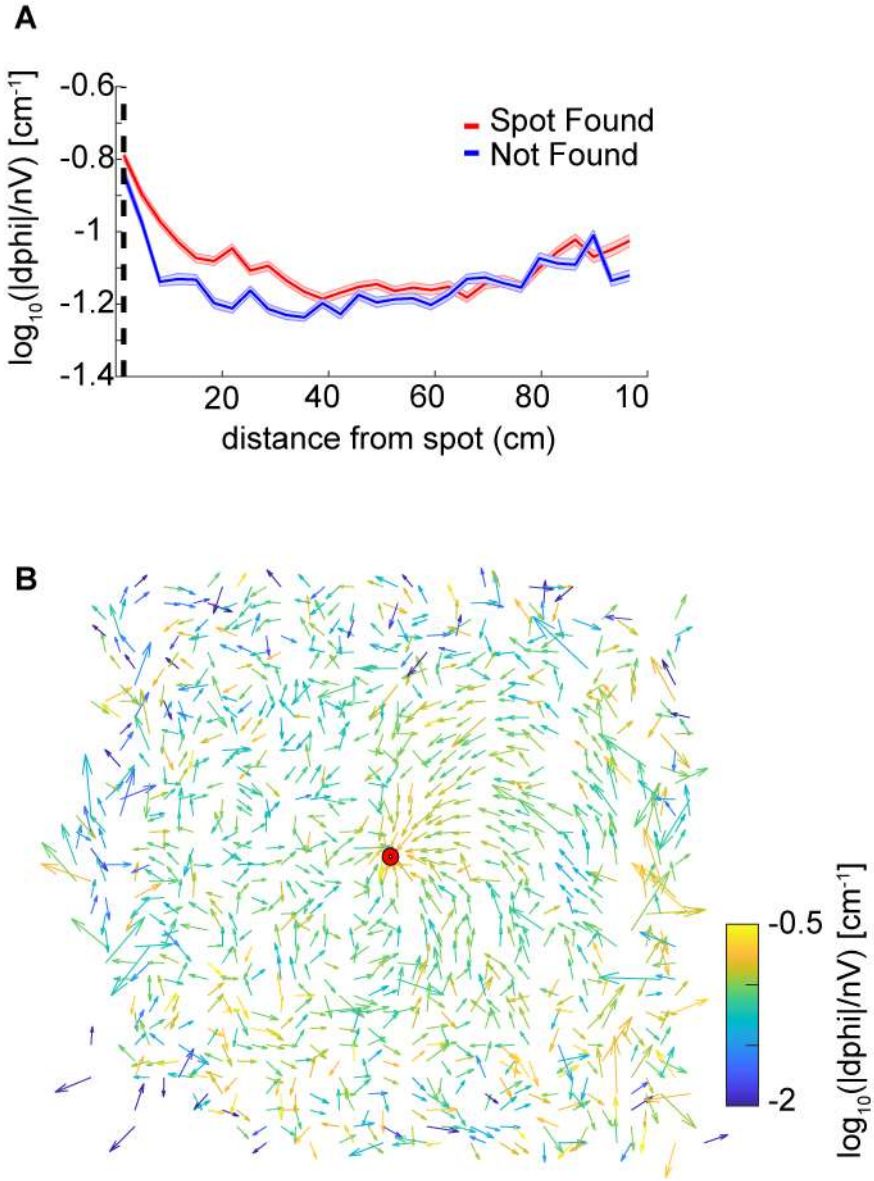

1154

1155

1156

1157

1158

1159

1160

FIGURE 5

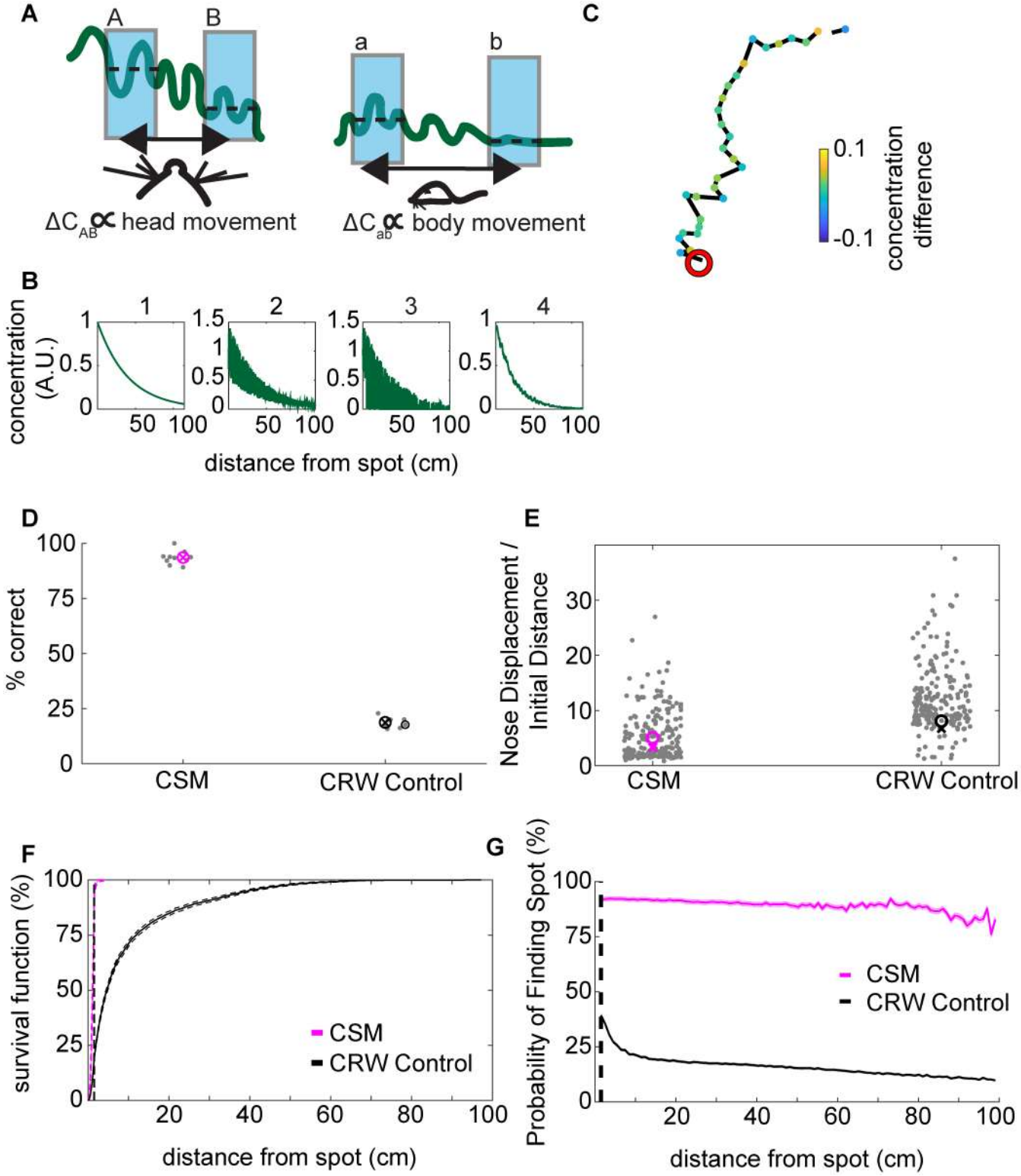
A
A
B
a
b
ΔC_AB ∝ head movement
ΔC_ab ∝ body movement
C
0.1
-0.1
concentration difference
B
concentration (A.U.)
1
2
3
4
distance from spot (cm)
D
% correct
CSM
CRW Control
E
Nose Displacement / Initial Distance
CSM
CRW Control
F
survival function (%)
CSM
CRW Control
distance from spot (cm)
G
Probability of Finding Spot (%)
CSM
CRW Control
distance from spot (cm)

1166

1167

1168 **FIGURE 6**

1169

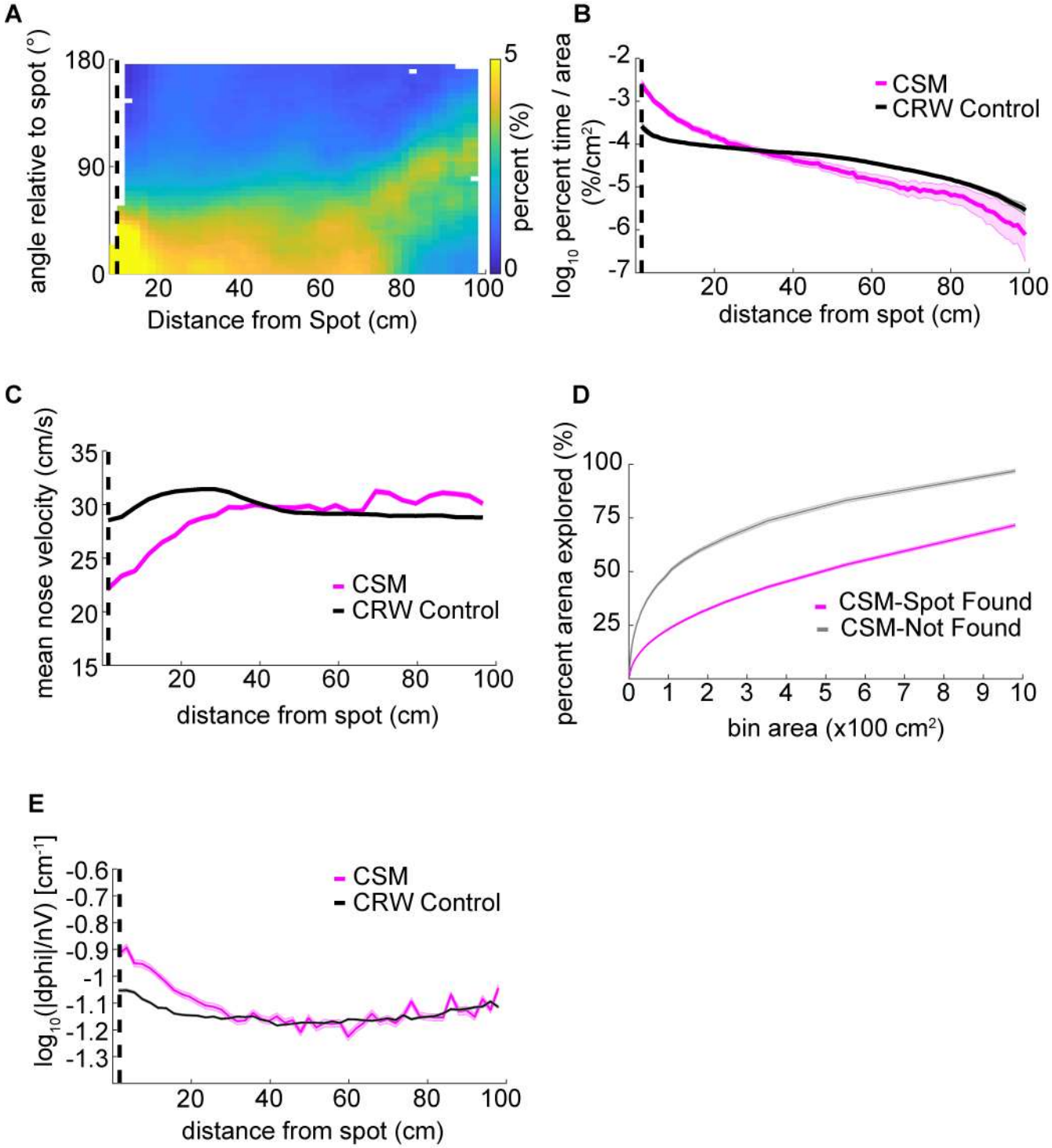

1170

1171

1172

FIGURE 7

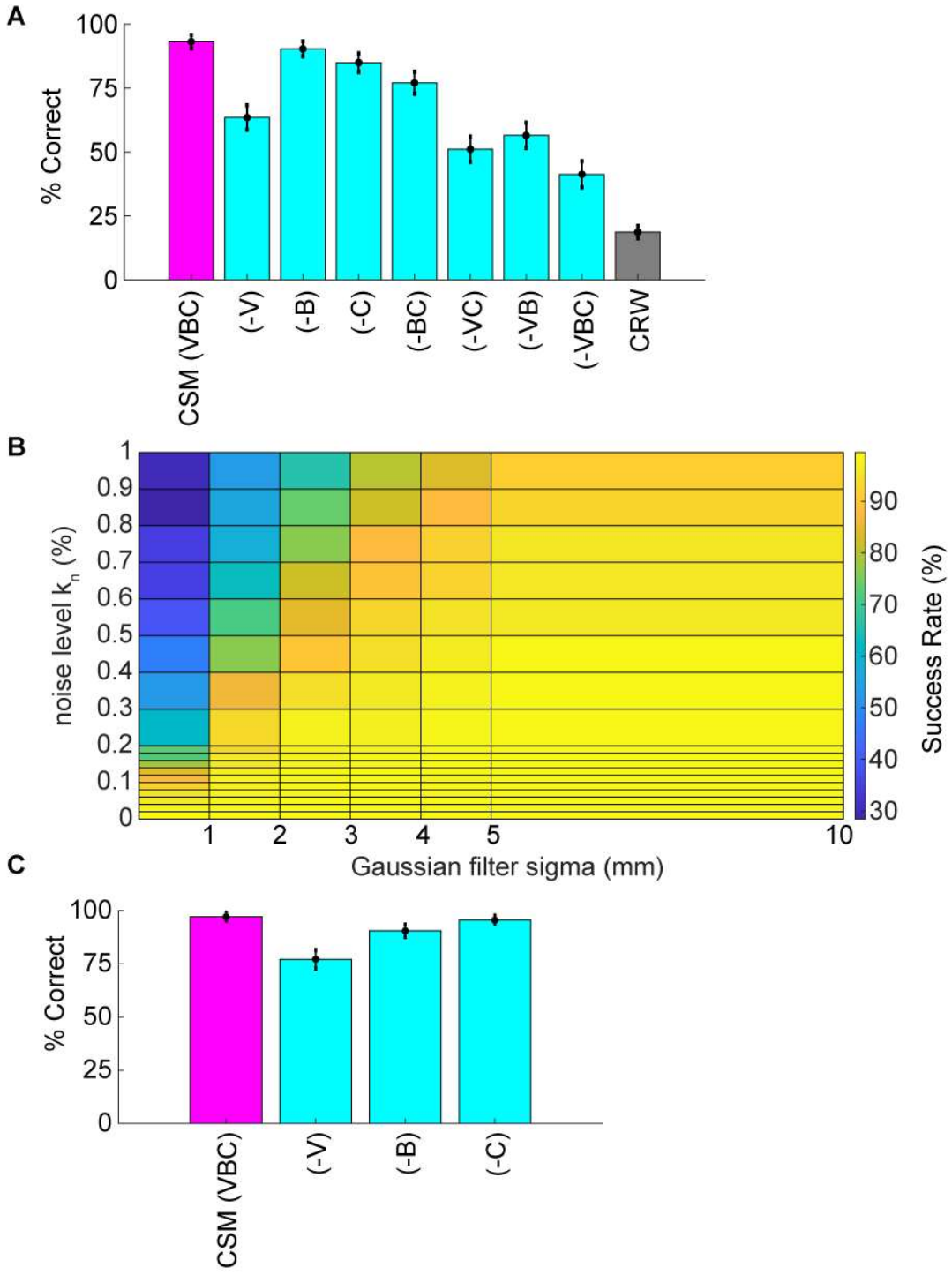
A
% Correct
100
75
50
25
0
CSM (VBC)
(-V)
(-B)
(-C)
(-BC)
(-VC)
(-VB)
(-VBC)
CRW
B
noise level k_n (%)
1
0.9
0.8
0.7
0.6
0.5
0.4
0.3
0.2
0.1
0
1
2
3
4
5
10
Gaussian filter sigma (mm)
Success Rate (%)
90
80
70
60
50
40
30
C
% Correct
100
75
50
25
0
CSM (VBC)
(-V)
(-B)
(-C)

1176

1177 **SUPPLEMENTAL FIGURE 1**

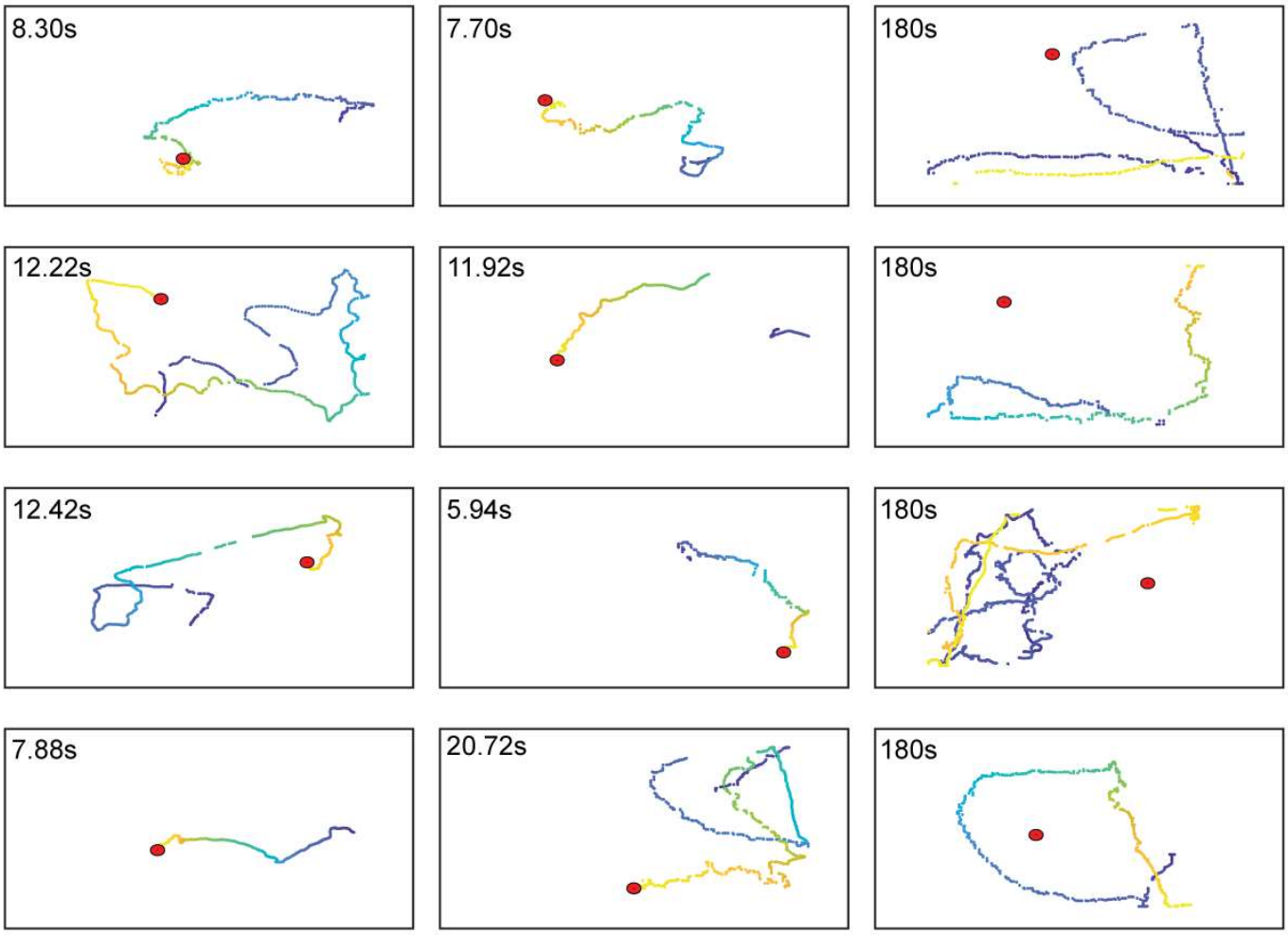

1178
1179
1180
1181
1182
1183
1184
1185
1186
1187

1188

1189 **SUPPLEMENTAL FIGURE 2**

1190

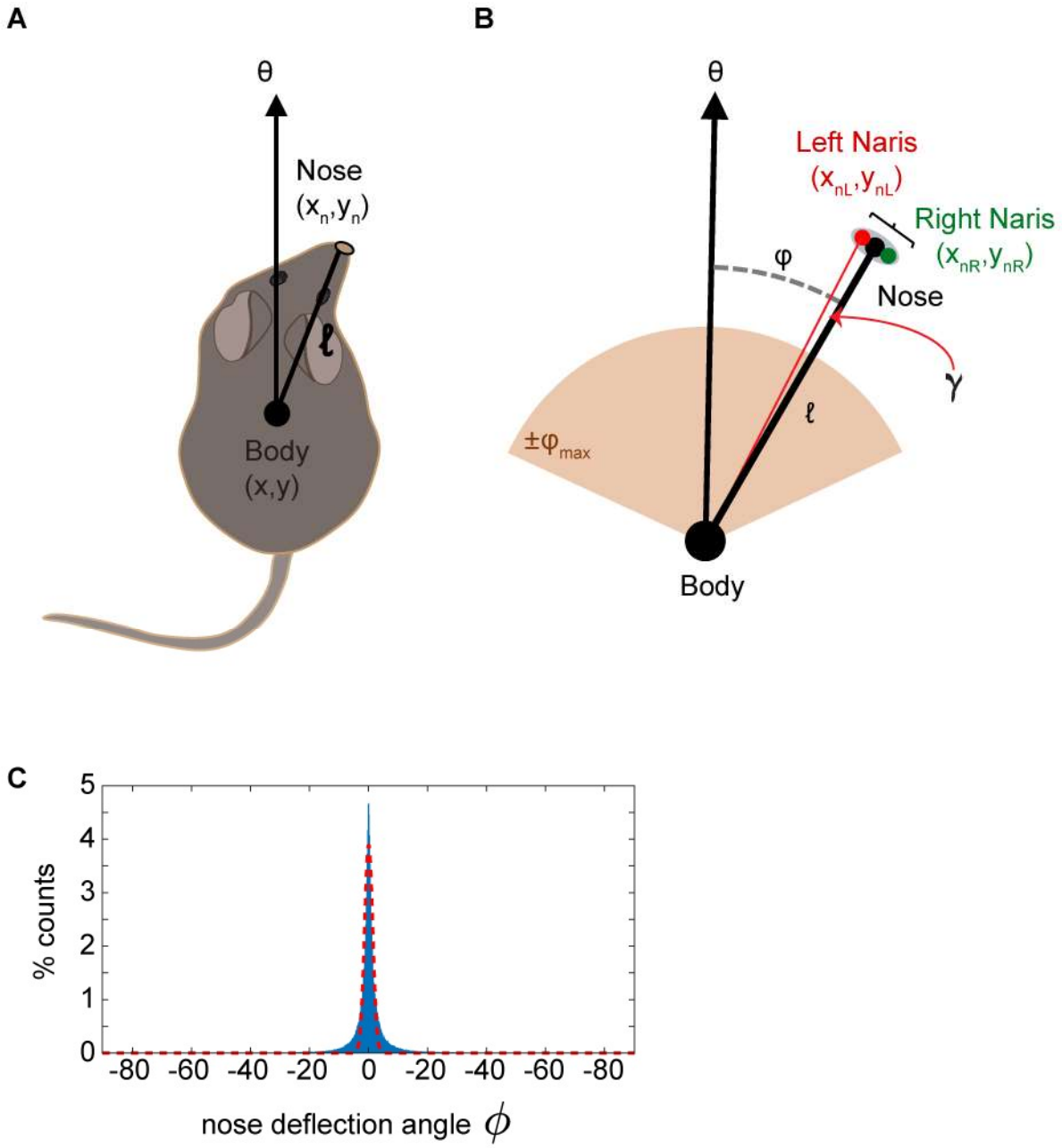

1191

1192

1193

1194

1195 **SUPPLEMENTAL FIGURE 3**

1196

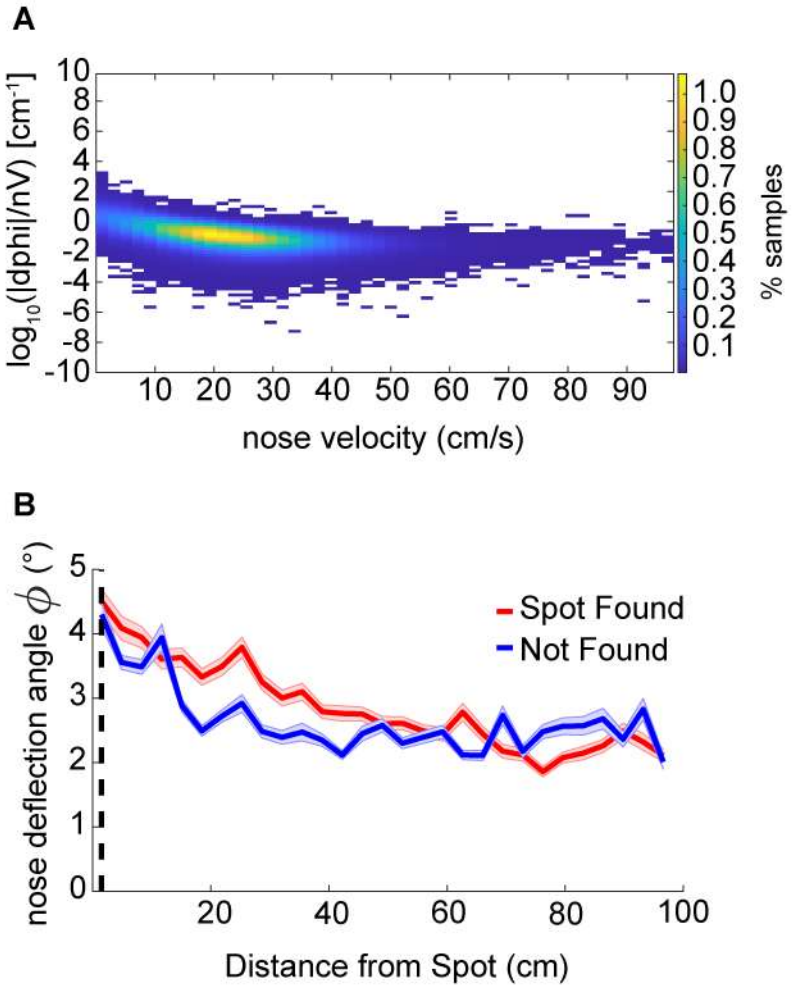

1197

1198

1199

1200 **SUPPLEMENTAL TABLE 1**

Variable	p value	β value
Experimenter	4.20E-01	-0.43
Baited	**4.68E-12**	**2.51**
Concentration	4.93E-03	0.56
Order of Trial	0.08	0.23
Trial	0.98	4.47E-03
Mouse	0.11	**0.16**
Initial Distance	**6.54E-08**	**4.53E-02**
Initial Orientation	0.79	3.26E-04
Mean Body Velocity	**6.89E-06**	**-0.29**
Mean Nose Velocity	**1.07E-04**	**0.27**
Displacement Ratio	**4.19E-19**	**-0.38**
Mean Curvature	**2.56E-03**	**1.4**
Exploration %	**1.65E-15**	**15.51**
Mean Nose Acceleration	0.01	-0.05
Time Stopped	0.22	-0.02

1201

1202

1203

1204

1205

1206

1207

1208

1209

1210

1211

1212

1213

1214

1215

1216

1217

1218 **SUPPLEMENTAL TABLE 2**

Variable	p value	β value	Range
d_{nares}	**1.00E-50**	**0.54**	**0.01 - 1cm**
k_c	4.84E-03	-0.1	0 - 1
$k_{binaral1}$	**6.86E-26**	**1.27E-03**	**0.01 - 300**
$k_{binaral2}$	**7.33E-106**	**0.16**	**0 - 5**
k_v	**2.63E-47**	**0.62**	**0 - 1**
ℓ (neck length)	**1.35E-191**	**0.26**	**0.01 - 10cm**
Mean Curvature (dist < 30cm)	**6.13E-09**	**0.6**	**Dependent Variable**
Mean Nose Velocity (dist < 30cm)	**2.30E-19**	**-0.016**	**Dependent Variable**
n_c	**4.67E-09**	**-0.043**	**0 - 5**
n_v	**4.76E-160**	**0.22**	**0 - 5**
σ_{max}	**1.11E-39**	**0.77**	**0.01 - 1**
σ_{min}	2.50E-01	0.074	0.01 - 1
τ	6.40E-01	-0.02	0.01 - 1
V_{max}	**9.26E-54**	**0.03**	**20 - 40cm/s**

1219